DEUTSCHES ELEKTRONEN-SYNCHROTRON DESY

DESY SR-72/7
June 1972

The Optical Properties of Dilute Solid Rare Gas Alloys in the Extreme Ultraviolet

by

R. Haensel, N. Kosuch, U. Nielsen, B. Sonntag
II. Institut für Experimentalphysik der Universität Hamburg, Hamburg, Germany

U. Rössler
Fachbereich Physik der Universität Marburg, Marburg, Germany

2 HAMBURG 52 · NOTKESTIEG 1

To be sure that your preprints are promptly included in the HIGH ENERGY PHYSICS INDEX, send them to the following address (if possible by air mail):

DESY
Bibliothek
2 Hamburg 52
Notkestieg 1
Germany

Deutsches Elektronen-Synchrotron DESY, Hamburg

The Optical Properties of Dilute Solid Rare Gas Alloys in the Extreme Ultraviolet

R. Haensel[+], N Kosuch[+], U. Nielsen[+], U. Rössler[‡], and B. Sonntag[+]

The absorption spectra of thin films of alloys of the rare gases Xe, Kr, Ar, and Ne have been measured in the photon energy range 40 to 260 eV, i.e. in the region of Ne 2s, Ar 2p, Kr 3d, and Xe 4d transitions. In most cases a continuous shifting of the energetic position of the absorption peaks of the pure rare gas solids upon addition of another rare gas or of N_2 can be observed, thus indicating a dilute alloying of both components over the whole range of concentrations. The shift of the absorption peaks can be understood in terms of the conduction band density of states of pure rare gas solids.

[+] II. Institut für Experimentalphysik der Universität Hamburg, Hamburg, Germany

[‡] Fachbereich Physik der Universität Marburg, Marburg, Germany

I. Introduction

In the past few years the investigation of the optical properties of solid rare gases in the extreme ultraviolet[1-4] has gained much interest. Since the rare gases can be studied in a relatively easy way, both in the gaseous and in the solid state, common and different features of the optical properties of both states can be disentangled by comparing the spectra over a wide spectral range. The optical spectra of gaseous and solidified rare gases have common extended maxima, which are typical for the continuum absorption but differ in the fine structure at the threshold energies where electrons from the different core shells can be excited.

The continuum absorption of rare gases, with a broad maximum typical at energies several ten eV above the threshold energy (delayed d→f transitions) is well understood with the help of atomic theories. Photoionization cross-sections, as calculated from realistic Hartree-Fock potentials for a single particle model[5-7], gave a good qualitative description of the experimental results. Recent calculations[8-11], that include exchange and correlation terms have improved agreement between the atomic model and the experiment. The characteristics of the continuum absorption have also recently been explained, from a solid state point of view[12], as being due to a lack of orthogonalization corrections on the dipole matrix elements for d→f transitions.

The fine structure in the optical spectra of solid rare gases at the onset of transitions from the valence band has been studied for several years[13-16]. Experiments, that have been performed with the help of LiF substrates[13-15], were restricted to photon energies smaller than 10.5 eV, because of the short wave-length cut-off of this material. This restriction was overcome by Baldini[16], who used a cooled sapphire rod coated with a phosphor for the detection of

ultraviolet light and directly evaporated the solid rare gas films onto this rod. He extended the accessible energy range up to 14 eV, the limit being due to his radiation source. The energy range was finally extended to 500 eV using synchrotron radiation as an ultraviolet source[17,18]. Besides transitions from the valence bands[19-21] transitions from different core shells have also been studied[1-4,22,23]. Additional absorption measurements on solid Ne have been performed between 17 and 21 eV in the region of the valence band transitions by Boursey et al.[24] using a triggered vacuum spark uranium rod source[25]. In the hard X-ray region the K-absorption spectra of solid Ar and Kr have been measured by Soules and Shaw[26]. Besides the optical measurements energy loss experiments have been performed[27-32].

An interpretation of the fine structure at the onset of transitions from the valence shell has been attempted in connection with energy band calculations for solid rare gases carried out by several authors[33-42]. In these interpretations the general custom is to ascribe structures in the absorption spectrum to critical points in the joint density of valence and conduction band states. This procedure, which is very useful in the interpretation of optical spectra of semiconductors, is not quite correct in the case of insulators. As the valence electrons are tightly bound to the ions (the gap energy in solid rare gases being of the order of 10 eV), the electrons are not able to screen the Coulomb interaction between the excited electron and the hole which it leaves behind in the valence band. Thus, excitonic structures due to bound states of the electron-hole pair appear as hydrogen-like series[43] in front of the interband continuum. In addition, the Coulomb interaction is responsible for fluctuations in the density of states continuum[44]. It has, however, been pointed out that the density of states curves of the conduction bands[45] are useful in the interpretation of the fine structure in the absorption curves at the onset of core shell transitions[1-4].

A study of the absorption spectra of solid solutions of rare gases in the extreme ultraviolet yields a further check on the interpretation given to these spectra of pure solid rare gases and thus promotes the understanding of core transition spectra in terms of electron states. Preliminary results of such experiments have already been reported elsewhere[2-4]. The measurements, discussed in this paper were performed on binary alloys of all rare gases and of N_2 for different concentrations c of the constituents. The energy range was between 40 and 260 eV. Since in this range all rare gases show not only core transitions but also continuum absorption from valence band an outer s-shell transitions effects cannot be seen for atomic impurities ($c < 1^o/oo$).

Atomic impurity absorption effects have been studied in the long wavelength region where the host crystal (e.g. Ar doped with Xe) is still transparent[13,46]. Some properties of the conduction band of the host crystal can be studied from the energy position of the exciton absorption lines. Other measurements on mixed systems with different concentrations have been performed on the solid rare gases in the valence band absorption region[47] and on the alkali halides in the valence band[48] and in the core transitions region[49]. They have been discussed with regard to the nature of absorption peaks as excitons and interband transitions coupled to different points of the Brillouin zone.

In the following section we will give some details of the experimental procedure, section III summarizes the experimental results and the last section will give a discussion of our results. We will present results of

a) the Xe 4d absorption in Xe:Kr mixtures
b) the Kr 3d absorption in Kr:Xe mixtures
c) the Xe 4d absorption in Xe:Ar mixtures
d) the Kr 3d absorption in Kr:N_2 mixtures
e) the Kr 3d absorption in Kr:Ar mixtures
f) the Ar 2p absorption in Ar:N_2 mixtures
g) the Ne 2s absorption in Ne:Ar mixtures

II. Experimental Details

The experimental setup is essentially the same as was used for the thin film absorption measurements of the pure rare gas solids[1,2]. It is described, to some extent, in ref. 1. Thin film absorption is the best method for obtaining optical constants in the energy range above 25 eV. The reflectivity in this energy range is very low and as a result no correction for reflection losses is necessary.

The light comes from the 7.5 GeV electron synchrotron DESY[17,18]. The spectrometer used for our experiments was a 1 m Rowland type spectrometer with grazing incidence. Two different gratings were used for the experiments: in the energy region between 60 and 100 eV a 2400 lines/mm grating yielded an energy resolution of $\sim$0.05 eV; at higher energies a 3600 lines/mm grating with an energy resolution of $\sim$0.2 eV was used. The radiation detector behind the exit slit was an open magnetic type photomultiplier (Bendix M 306). No absolute absorption values have been obtained because the thickness of the thin filmswas never determined. The relative accuracy of the measurements allowed us to detect changes of more than 3 % in the absorptivity of the samples. The energy calibration method based on wavelength values given for gas absorption lines is the same as was used in ref.s 1 and 2. The resulting energy positions for the peaks in pure rare solids are slightly different from the values previously found[1,2], but are in agreement within the error limits.

The gas mixtures were evaporated in <u>situ</u> onto thin foils which are mounted on a cryostat installed between the source and the spectrometer. The mixtures were prepared by putting the appropriate amounts of the constituents in a stainless steel pipe, the amounts were controlled by measuring the total pressure with a precision membrane vacuummeter (Datametrix Model 1014). Circulation in the pipe was necessary in order to completely mix the constituents. The mixtures

were evaporated at temperatures below the sublimation temperature of both constituents ($\sim$45° K for Xe, $\sim$40° K for Kr, $\sim$20° K for Ar, and $\sim$7° K for Ne) and it is assumed that the composition in the solid phase was the same as in the gas phase before evaporation. As a result the values later used for the composition of the rare gas alloys are the relative partial pressures of the total pressure of $\sim$760 Torr in the mixing vessel before evaporation. The substrates were thin films (of the order of 100 to 1000 Å thickness) of Al, Mg and C. Al and Mg also served as prefilters to suppress higher order stray light.[50]

We studied the Xe 4d absorption between 65 eV and 90 eV with admixtures of Kr and Ar, the Kr 3d absorption between 90 eV and 100 eV with admixtures of Xe, N_2, and Ar, the Ar 2p absorption between 243 eV and 255 eV with admixtures of N_2, and the Ne 2s absorption between 45 eV and 49 eV with admixtures of Ar. Fig. 1 shows the absorption curves of pure solid Ne, Ar, Kr and Xe in the energy region between 25 eV and 350 eV. We see that in the fine structure region of the Ne 2s, Xe 4d, Kr 3d, and Ar 2p transitions the other gases generally show a smooth continuum absorption. This is also true for N_2 over the whole energy range.[51]

If two gases would not form a dilute alloy but a solid with well separated regions of the two components pure additive superposition of the two absorption curves would occur and the energy position of the absorption peaks in fine structure regions would essentially be unaffected. We will, however, later see that for many cases the absorption peaks are continuously shifted from the position in the pure material to higher or lower energies depending on the second component and the mixing ratios in the alloy. This fact indicates a complete alloying of the two components through the whole range of mixing ratios.

The dilute alloying was also observed in electron diffraction patterns of mixed solid rare gas films. The diameters of the different rings in the diffraction pattern showed a smooth transition between the values of the pure components which formed the alloys.

Only a few cases, namely Xe:Ar and Kr:N_2, were observed where, for certain concentrations, no complete alloying occured. This was observed from the fact that the absorption peaks were found at the positions in pure Xe or Kr resp. (for details see section III).

In the electron diffraction studies we found no evidence of monocrystal structure in portions of our samples; the area of diffraction, however, was relatively large ($\sim$0.5 mm^2). We know that the optical structure, i.e. the width of the sharpest peaks depends on the temperature during evaporation[1]. At temperatures just below the sublimation temperatures we obtained peaks widths which were the same as the widths of the corresponding gas absorption lines. We therefore assumed that the crystalline order was sufficient to obtain optimal line widths.

As we have mentioned before the sublimation temperature for pure Xe samples is 45° K, but for Xe:Kr one has to evaporate below 40° K and for Xe:Ar mixtures below 15° K. To see the effect of temperature in pure Xe samples these were also studied at different temperatures between 40° K and the temperature of liq. He. Evaporation at lower temperatures increases the line width, but the peak maxima can still be observed and their positions do not change when the evaporation temperature is varied.

The experimental results of the different absorption measurements are given in Fig.s 2 - 10. The absorption curves have been obtained by dividing the trans-

mission curves of the evaporated and the empty substrates. The final curves have been obtained from absorption curves derived from measurements with films of different thickness. This also served to check the consistency of the results. The zero of absorption has been suppressed and the absorption values are given in arbitrary units since absolute values are of no importance for the problems now under consideration. We are mainly interested in the shape and energetic positions of the different absorption maxima. For this reason the influence of stray light and higher orders was also of minor importance; both, however, were kept low by appropirate filtering with Al- and Mg-foils.

III. Experimental Results

In this section we are going to present the experimental results given in Fig.s 2 - 10.

a) Xe 4d structure in Xe:Kr mixtures

Fig. 2 shows the fine structure of the Xe 4d absorption in the energy range between 64 and 90 eV for different Xe:Kr alloys with Xe content ranging from 100 % to 1 %. Even for 1 % Xe some structure can be seen because in this range the ratio of Xe and Kr absorption is especially favourable (see Fig. 1, where σ of Xe in the region of 4d fine structure is $\sim$6 Mb, whereas σ for Kr in the same energy range is $\sim$0.7 Mb). The labelling of the peaks A, B, B' ... H, H' is the same as in ref. 1. We see that by adding Kr all the peaks move to higher energies, the more the higher their energies are above threshold ($\sim$65 eV). No shift is observed for A, the shift of H' is about 2 eV. An exception to this rule is the peak J near 80 eV which shows no shift when adding Kr. With the exception of low Kr contents (C_{Kr} <20 %) the shift of the energy positions is proportional to the Kr concentration.

Fig. 3 shows the energetic positions of the different maxima as taken from the original curves for the different Xe:Kr concentrations. The absorption spectra show transitions from the different sublevels ($J = \frac{5}{2}$ and $\frac{3}{2}$) of the Xe 4d level, which have an energy distance of $\sim$2 eV.[52] The corresponding peaks have the same primed and unprimed roman letter. The gradient of $\frac{\Delta E}{\Delta c}$ depends on the energy of the peak in pure Xe, but we find the same gradient for the corresponding peaks. This supports the former assumption[1] that they are corresponding spin-orbit mates. In ref. 1 the assignment of spin-orbit mates has come from their energy separation of $\sim$2 eV and the similarity of their shapes. We now have the additional information that spin-orbit mates are shifted by the same amount by alloying another rare gas. The linear dependence

of the peak shift on the Kr concentration allows extrapolation to $c_{Xe} = 0$ % or $c_{Kr} = 100$ % resp. The position of the Xe 4d peaks in 100 % and 0 % Xe is summarized in Table I. The energy shift obtained by this extrapolation procedure will be called "maximum shift" for all the alloys reported in this paper. We very clearly see that the energy shift is the same for the corresponding spin orbit partners.

The fact that at certain energies peaks may be seen which result from the superposition of transitions from different spin-orbit subshells of 4d (with J = 5/2 and 3/2) consequently having different $\frac{\Delta E}{\Delta c}$ explains the disappearence of e.g. the faster moving peaks E, F under the slower moving peak B'. The different $\frac{\Delta E}{\Delta c}$ within one series also explains why C, being more a shoulder of D in pure Xe, becomes more distinguishable from D with higher Kr concentrations. The same is true for C' and D'.

The situation is more entangled for C' and D'. We have to consider that the structure C', D' has contributions from different conduction band density of states.[45] It is, therefore, difficult to exactly determine the maximum shift of D' (see Table I).

b) Kr 3d structure in Kr:Xe mixtures

Fig. 4 shows the fine structure of the Kr 3d transitions between 91 and 99 eV for different Kr:Xe concentrations. In contrast to the Xe 4d structure we here see a shift to lower energies when Xe is added. The shift is small near the onset of transitions (B and B', which again show the same behaviour as the other spin orbit mates) and becomes larger for peaks at higher energies (e.g. G, G') so that the whole spectrum tends to contract, whereas the Xe 4d spectrum in Xe:Kr mixtures expands.

The situation for identifying peaks and for following their motion to lower Kr concentrations is less favourable than for the Xe 4d spectrum in the Xe:Kr mixtures: α) As can be seen from Fig. 1 the Xe absorption near 90 eV has merely a broad maximum with $\sigma \simeq 27$ Mb, whereas the Kr 3d fine structure ranges between 0.7 and 3 Mb. It is, therefore, difficult to observe the Kr 3d structure for small Kr concentrations. β) As the whole spectrum contracts and the spin orbit splitting energy of the Kr 3d shell is less than that of Xe 4d, namely $\sim$1.2 eV,[52] the peaks are not so well separated from each other.

In Fig. 5 the peak positions for the different Kr:Xe concentrations are taken from the original spectrometer curves. We see that with the reserved sign $\frac{\Delta E}{\Delta c}$ increases again when going to higher energies. The extrapolation to 0 % Kr giving the values for the maximum shift, summarized in Table II, obviously contains a larger error than the Xe values in Table I.

c) Xe 4d structure in Xe:Ar mixtures

The fine structure of the Xe 4d absorption in the energy range 64 and 80 eV is shown again in Fig. 6 but now with alloying solid Ar. As for Xe:Kr mixtures we see a shift of the peaks to higher energies. A breaking of the systematic shift seems to occur in the curve with $c_{Xe} = 60$ %. At the energy position of H in pure Xe a peak occurs which obviously indicates at least a partial dealloying of the two components. Table I also shows the energetic positions of the different peaks for $c_{Xe} = 0$ % ($c_{Ar} = 100$ %) as obtained from the original spectrometer curves. We again find a shift proportional to the Ar content for $c_{Ar} > 20$ % (see Fig. 6).

A comparison of the values given in Table I shows that the shift of peaks is much larger for Ar alloys than for Kr alloys. Peak A does not shift in both

cases, but for B (B') the shift is 0.17 eV (0.16 eV) in Kr and 0.58 eV (0.58 eV) in Ar, for C (C') the shift is 0.28 eV (0.25 eV) and 0.75 eV (0.80 eV) resp., and finally for H (H') and I we obtain 2.02 eV (2.04 eV) and 2.06 eV for Kr and 3.2 eV (3.2 eV) and 3.2 eV for Ar.

It should, however, be noted that an unambiguous association of the corresponding peaks of different concentrations is much easier in the Xe:Kr system than in the Xe:Ar system. The shift of the B, B', C, C' structures in Xe:Ar is quite clear but for the higher energy peaks G, H and H' one could also think that for c_{Ar} = 40 and 90 % they are at just the same position as in pure Xe. This could be explained by a demixing of the system for these concentrations, but if this is so, the peaks B, B' should also be at the position in pure Xe, which is obviously not the case.

d) Kr 3d structure in Kr:N_2 mixtures

A clear case of de-alloying can be observed in the Kr:N_2 mixture (Fig. 7). For small N_2 concentrations one sees that the different peaks shift to higher energies, but for 40 % and more the Kr peaks appear again at their old positions. Here the Kr and N_2 obviously form well separated islands in the film.

e) Kr 3d structure in Kr:Ar mixtures

Fig. 8 shows the fine structure of the solid Kr 3d absorption in the energy range 90 to 100 eV with the alloying of Ar. We again find the general tendency that the peaks are shifted to higher energies. The peak shift increases the higher the peak position above threshold. Table II shows the energetic positions of the different peaks for c_{Kr} = 0 % (c_{Ar} = 100 %) as obtained from the original spectrometer curves. The shift is once more proportional to c_{Ar}, and $\frac{\Delta E}{\Delta c}$ is again the same for spin orbit mates. The structures above 96 eV were only observable

up to $c_{Kr} \simeq 50$ to 60 %. It seems that two of the peaks, namely J and L split into two peaks. The explanation may be that they are composed of transitions from the different Kr 3d subshells which both shift with different amounts. The splitting of L may also be due to the fact that L is partially caused by a double excitation (see Section IV. c).

The broad structures near 110 eV could be observed up to 80 % Ar. They shift much less than peaks at lower energies, as is also the case for the structures in Xe at 80.0 eV.

Another interesting feature is that the peaks B, B', C and C' become more and more pronounced if Ar is added.

f) Ar 2p structures in Ar:N_2 mixtures

The 2p absorption of solid Ar has been investigated in mixtures with Kr, Xe and N_2. In Ar:Kr and Ar:Xe the peaks shift to lower energies, with N_2 they shift to higher energies. Fig. 9 shows the fine structure in the energy range 243 eV to 255 eV with alloying of N_2. The results have already been mentioned in ref. 2. In the pure Ar spectrum the spin orbit mate of A labeled A' can only be seen as a shoulder of B. When alloying N_2 the peaks A and A' do not change their position at 245.3 and 247.5 eV, whereas B at 248.0 eV is shifted by +1.0 eV and B' at 250.0 eV by +1.2 eV. Thus A' and B can be seen as clearly separated maxima in the Ar:N_2 mixtures.

g) Ne 2s structures in Ne:Ar mixtures

We would finally like to mention the results of Ne:Ar alloys. Fig. 10 shows the fine structure of the solid Ne 2s absorption in the energy range 45.5 to 48.5 eV with alloying of Ar. The lines in pure solid Ne have a strongly asymmetric shape,[23] very similar to what has been found in the gas.[53] In the

Ne:Ar alloys the peaks are shifted to lower energies but the line profile character remains unchanged. Extrapolating to c_{Ne} = 0 % (c_{Ar} = 100 %) gives a maximum shift for the first line at 46.92 eV in pure Ne by -0.5 eV and for the second line at 48.0 eV in pure Ne by -1.1 eV.

Here is a summary of the experimental results:

a) The different absorption peaks shift when other gases are added.

b) If the atomic number of the admixed gas is higher the peaks shift to lower energies, if the atomic number is lower the peaks shift to higher energies.

c) The energy shift of the absorption maxima are almost proportional to the concentration of the admixed partner.

d) The amounts of energy shifting are small near threshold and increase the larger the distance of the maxima from threshold. Spin orbit mates shift equally. The first peaks show an additive shift, that means e.g. Ar shifts the Xe peaks by an amount (see Table I), which is approximately the sum of the Xe shift by Kr (Table I) and the Kr shift by Ar (Table II).

IV. Discussion

Before we go into a detailed discussion on the alloy measurements of Section III we have to review some facts which have already been discussed in connection with the experimental data of the pure solid rare gases.[1-4,45]

With the exception of some lines (A and B in the Ne 2s and Ar 3s spectra and B and C in the Kr 3d and Xe 4d spectra) near the onset of transitions from the core shell the absorption spectra can be explained as being due to density of states structures. These first lines, due to their energetic position close to the first gas absorption lines, their line shape and width comparable to that of the gas lines, can be interpreted as Frenkel excitons. Since, to some extent, the reaction of these excitonic peaks to alloying is different from that of density of states structures, we are going to discuss excitonic and density of states effects on the optical spectra of solid rare gas alloys separately.

a) Excitonic effects (transitions near threshold)

Fig. 11 shows the absorption curve of gaseous and solid Ne 2s, Ar 3s and 2p, Kr 3d, and Xe 4d transitions in the vicinity of the first gas lines. The energy scales of the different spectra are normalized at the first gas line. The energy positions of the gas and solid state absorption lines and their relative distances are compiled in Table III. In all spectra the first strong absorption line in the solid (A in Ne and Ar, B in Kr and Xe) is at higher energies than the first gas line. By comparing the experimental spectra with the calculated curves for the joint density of states[45] we conclude that the Frenkel excitons in Kr 3d and Xe 4d are above the interband transition threshold. This conclusion is supported by the fact that the oscillator strength of these excitons in Kr and Xe is smaller than that of the corresponding gas lines due to interactions

with the underlying continuum. Peak A in Ar 2p, corresponding to a Frenkel exciton built from a 2p-hole and an s-symmetric electron, is below the onset of interband transitions and in contrast to B in Kr and Xe its oscillator strength is similar to that of the gas line. For Ne 2s and Ar 3s only the first two or three lines can be observed experimentally. No further structure, which could be compared with the density of states curve can be seen. Therefore, it is hard to decide whether these peaks are below or above threshold. This complete lack of interband transitions in the experimental curves of Ne 2s and Ar 3s transitions remains to be explained.

We now compare the position of the first solid state absorption line (A, A' in Ne and Ar; B, B' in Kr and Xe) with the position of the gas line for the case that in the solid the excited atom is surrounded by atoms of the same element (pure solid) or by atoms of a different rare gas (alloys). In Fig. 12, on the left, we see the energy distance of the Xe 4d lines B and B' to the gas lines when the Xe atom is imbedded in Xe, Kr and Ar. The energy distances are taken from Tables I and III. Further to the right in Fig. 12, for Kr 3d, we see the energy distance to the first Kr 3d gas lines for Kr in Xe, pure Kr and Kr in Ar, as taken from Tables II and III. For Ar 3s only the distance from the gas line to the pure solid is included as no alloy measurements have been performed for this transition. For Ar 2p the distance is included for Ar in Xe, Ar in Kr and pure Ar (Table III and data not included in Section III) and finally for Ne 2s the distance for Ne in Ar and pure Ne (see values in Section III and Table III).

The result is that the relative position of the first solid state absorption line depends only on the neighbouring atoms and not on the isolated atom from which the transition comes. E.g. the distance of the first Frenkel exciton in

solid Ar from the gas line is ∿0.9 eV both for 2p and 3s transitions. The same value is found for the first Frenkel exciton in the 4d spectrum of Xe imbedded in Ar from the Xe gas line.

A similar result is found for the separation of the first two absorption lines in the solid, namely B - A in Ne and Ar, C - B in Kr and Xe for the pure and alloyed solids (Fig. 13). On the left, for Xe 4d, we see the distance C - B for pure Xe and for Xe in Kr and Xe in Ar, to the right follows Kr in Xe, pure Kr and Kr in Ar, then pure Ar 3s and finally Ne in Ar and pure Ne. We once more see that the energy distances of the first two absorption lines of a solid are only dependent on the neighbouring atoms and not on the excited atom. The data given in Table III and Fig. 12 show that the blue shift of the first exciton with respect to the corresponding gas line increases when going from Xe to Ne. In the same way the separation of the first two exciton lines increases (Fig. 13).

Kozlenkov[54] and Kronig[55] made theoretical calculations for metal and metal alloys on the energy shift of absorption maxima with changing lattice constant a. According to these theories the shift should be proportional to $1/a^2$. Assuming $a_{Ne} = 4.465$ Å, $a_{Ar} = 5.315$ Å, $a_{Kr} = 5.654$ Å and $a_{Xe} = 6.136$ Å one can plot E against $1/a^2$ (Fig. 14). We see that the proportionality also holds true for the solid rare gases.

b) Density of states effects

The concept underlying the study of density of states effects on the optical spectra of solid rare gases in the far ultraviolet is the calculation of the dielectric constant in the simplified from

$$\varepsilon_2(E) \sim \frac{1}{E^2} \sum_{i,f} n_{fi}(E)$$

neglecting the energy and $\vec{k}$ dependence of the transition matrix elements. The point density of states

$$n_{fi}(E) = \frac{1}{N} \sum_{k \in BZ} \delta(E_f(\vec{k}) - E_i(\vec{k}) - E)$$

between initial core states (i) and final conduction bands (f) is just a replica of the conduction band density of states, because the core energy bands $E_i(\vec{k})$ do not depend on $\vec{k}$. For pure rare gas solids[45] it has already been shown that up to excitonic peaks (A, A' in Ar 3s transitions and B, B', C, C' in Kr 3d and Xe 4d transitions) all structures in the core excitation spectra correspond to density of states. This can be seen in Fig. 15 which contains the most important results of ref. 45. When discussing the effect of density of states on the optical spectra of dilute solid rare gas alloys in the extreme ultraviolet we will make use of our knowledge of the density of states in the pure crystals.

The Xe:Kr mixtures: As is shown in Fig.s 2 and 4 the structures D, E, F, G, H and their spin orbit partners shift with changing composition but do not split. They must be classified as amalgamation type structures[56] in agreement with their identification as density of states structures in the pure Xe or Kr spectrum.[45] Thus, what starts out as the pure Xe spectrum in the lowest curve of Fig. 2 should turn out more and more and become the pure Kr spectrum in the upper curve of Fig. 2, a spectrum which is to be understood in terms of the density of states structures of the Kr conduction bands. (Here of course the spin-orbit splitting of the Xe 4d as an initial state causes differences in the Kr 3d spectrum).

Since no density of states calculations are available for the mixed crystals a quantitative discussion of theoretical and experimental results is only

possible for the maximum shifts which are introduced in Tables I and II. If we assume that there is no shift of the core states with regard to the bottom of the conduction band a theoretical prediction of the maximum shifts for density of states structures follows by comparing the position of corresponding conduction band denstiy of states maxima in Xe and Kr with respect to the bottom of the conduction band. The theoretical shifts obtained in this way are given in Fig. 16 together with the experimental results.

The experimental values for the maximum shifts of the density of states maxima for the lowest conduction bands are taken from Tables I and II. Thus, the experimental maximum shift of the first conduction band is identical to that of D in Table I which was related to the maximum of the first conduction band density of states.[45] As we have already mentioned the maximum shift of D' is probably different from that of D because of contributions from the third conduction band density of states. E, F and E', F' have been interpreted as being due to the second conduction band density of states in Xe with E', F' also containing contributions from the fourth conduction band. Table I is also used to give the experimental maximum shift of the fifth conduction band density of states maximum (G). Since the density of states maxima of the third and fourth conduction band in Xe contribute to more complex structures the experimental maximum shifts can be more accurately obtained from Table II using the interpretation given for the Kr 3d spectrum. According to ref. 45 peaks F and G in Fig. 4 are built up by the third Kr conduction band density of states, whereas H and H' are caused by the density of states of the fourth conduction band of Kr.

Agreement between experimental and calculated maximum shifts of the five lowest conduction bands supports the previously given interpretation of the pure solid rare gas spectra by means of density of states structures. Following this concept we will now discuss:

The $Ar:N_2$ mixtures: The spectra of the $Ar:N_2$ mixtures with excitation from the Ar 2p level are presented in Fig. 9. Whereas in the pure Ar spectrum (lowest curve) two excitons A and A' and a variety of density of states structures (B, B', D, E, D') can be seen, the spectrum of the mixed crystal with c_{Ar} = 10 % (c_{N_2} = 90%) N merely shows two doubletts, A, A' and B, B'. In the pure Ar spectrum the excitonic peaks A and A' have been identified as being due to Frenkel excitons between the spin-orbit split 2p core states of Ar and the lowest conduction band. B and B' correspond to the density of states of the lowest conduction band and the higher energy peaks are related to the higher conduction bands in solid Ar[45] which correspond to atomic 3d levels. Although we have no detailed information on the band structure of solid N_2 we do know that energy band corresponding to atomic 3d states of N_2 must be high up in the conduction band and cannot be involved in that part of the spectra shown in Fig. 9. The lowest conduction bands of N_2 can be expected to have a structure similar to those of solid Ne.[39] This fully explains the simple spectra for high N_2 concentration in Fig. 9. Thus the upper spectrum can be interpreted as the spin-orbit split density of states structures B, B' corresponding to the lowest conduction band in N_2 and a pair of Frenkel excitons A, A' on Ar sites.

The Xe:Ar and Kr:Ar mixtures: The Xe:Ar and Kr:Ar mixtures (Fig.s 6 and 8) as was also the case with the Xe:Kr mixtures exhibit a widening of the spectra with increasing admixture of the lighter rare gas. In contrast to this the conduction band density of states does not follow this trend when going from Xe or Kr to Ar, e.g. the first and second density of states maxima are at lower energy in Ar than in Xe or Kr.[45] Thus, the concept which led to a sound interpretation of the Xe:Kr and $Ar:N_2$ spectra does not work here with the same success. Before we offer two possible interpretations of the spectra of Fig.s 6 and 8 we should mention that the shift of the higher peaks (E, F, G, H) in the Xe:Ar and Kr:Ar

mixtures cannot be followed as unambiguously as was possible in the Kr:Xe and Ar:N_2 mixtures.

On the Ar side the spectra in Fig.s 6 and 8 show a doublet which repeats itself at a distance equal to the core state spin-orbit splitting. The shape of these structures and their separation from each other and from the onset of core excitation bears some resemblance to the first and second conduction band density of states of pure Ar. The corresponding peaks in the pure Xe and Kr spectrum do not otherwise merge into these peaks on alloying, but, on the contrary move to higher energies.

On the other hand an explanation of the first peaks in the upper curves of Fig.s 6 and 8 by going back to B and C (B', C') in the pure Xe and Kr spectrum leaves us with the question of why the shape of the first (excitonic) peaks is so drasticly broadened on alloying.

c) Double excitations

We should finally like to briefly comment on the nature of the high energy structures J in Xe (Fig. 2) near 80 eV and L, M in Kr (Table II) near 110 eV. These structures do not shift at all upon alloying or shift by an amount much smaller than an extrapolation from the absorption lines behaviour at smaller energies would let one expect. These peaks have been assigned[1] as being due to a double excitation of the core shell d electron and a valence p electron in analogy to the interpretation of corresponding absorption lines in gaseous Xe and Kr at the same energy.[57] As for the double excitations the final states of both electrons are closer to the threshold, the small or zero shift has a natural explanation.

ACKNOWLEDGMENTS

Preliminary measurements of the Xe 4d absorption in Xe:Kr performed by P. Schreiber[3] led to the systematic studies of all mixtures described in this paper. The authors are grateful to G. Keitel for extended technical assistance and for valuable suggestions during the performance of the measurements. Thanks are also due to the Deutsche Forschungsgemeinschaft for financial support.

References

1. R. Haensel, G. Keitel, P. Schreiber, and C. Kunz, Phys.Rev. 188, 1375 (1969)
2. R. Haensel, G. Keitel, N. Kosuch, U. Nielsen, and P. Schreiber, J. de Physique 32, C4-236 (1971)
3. P. Schreiber, thesis, Universität Hamburg, 1970, internal report DESY F41-70/6 (unpublished)
4. G. Keitel, thesis, Universität Hamburg, 1970, internal report DESY F41-70/7 (unpublished)
5. J.W. Cooper, Phys.Rev. Letters 13, 762 (1964)
6. S.T. Manson and J.W. Cooper, Phys.Rev. 165, 126 (1968)
7. U. Fano and J.W. Cooper, Rev.Mod.Phys. 40, 441 (1968) and 41, 724 (1969)
8. W. Brandt, L. Eder, and S. Lundqvist, J. Quant. Spectrosc. Rad. Transf. 7, 185 (1967)
9. A.F. Starace, Phys.Rev. a 2, 118 (1970)
10. M.Y. Amusia, N.A. Cherepkov, and L.V. Cernysheva, Sov.Phys. JETP 33, 90 (1971)
11. D.J. Kennedy and S.T. Manson, Phys.Rev. A 5, 227 (1972)
12. Y. Toyozawa, Third Int. Conf. on VUV Rad. Phys. Tokyo 1971
13. K. Dressler, J. Quant. Spectrosc. Rad. Transf. 2, 683 (1962)
14. I.T. Steinberger, C. Atluri, and O. Schnepp, J.Chem.Phys. 52, 2723 (1970)
15. R. Scharber and S.E. Webber, J.Chem.Phys. 55, 3985 (1971)
16. G. Baldini, Phys.Rev. 128, 1562 (1962)
17. R. Haensel and C. Kunz, Z. Angew. Phys. 23, 276 (1967)
18. R.P. Godwin, in Springer Tracts on Modern Physics, Vol. 51, editor G. Höhler (Springer Verlag 1969) p. 1
19. R. Haensel, G. Keitel, E.E. Koch, M. Skibowski, and P. Schreiber, Phys.Rev. Letters 23, 1160 (1969)
20. R. Haensel, G. Keitel, E.E. Koch, M. Skibowski, and P. Schreiber, Opt.Comm. 2, 59 (1970)

21. R. Haensel, G. Keitel, E.E. Koch, N. Kosuch, and M. Skibowski, Phys.Rev. Letters 25, 1281 (1970)

22. R. Haensel, G. Keitel, P. Schreiber, and C. Kunz, Phys.Rev. Letters 22, 398 (1969)

23. R. Haensel, G. Keitel, C. Kunz, and P. Schreiber, Phys.Rev. Letters 25, 208 (1970)

24. E. Boursey, J.-Y. Roncin, and H. Damany, Phys.Rev. Letters 25, 1279 (1970)

25. H. Damany, J.-Y. Roncin, and N. Damany-Astoin, Appl.Opt. 5, 297 (1966)

26. J.A. Soules and C.H. Shaw, Phys.Rev. 113, 470 (1959)

27. E.M. Hörl and J.A. Suddeth, J.Appl.Phys. 32 2521 (1961)

28. O. Bostanjoglo and L. Schmidt, Phys.Letters 22, 130 (1966)

29. P. Keil, Z. Phys. 214, 251 (1968)

30. J. Daniels and P. Krüger, phys.stat.sol. (b) 43, 659 (1971)

31. C. Colliex and B. Jouffrey, J. de Physique 32, 46 (1971)

32. L. Schmidt, Phys. Letters 36A, 87 (1971)

33. R.S. Knox and F. Bassani, Phys.Rev. 124, 652 (1961)

34. W.B. Fowler, Phys.Rev. 132, 1591 (1963)

35. L.F. Mattheis, Phys.Rev. 133, A1399 (1964)

36. M.H. Reilly, J.Phys.Chem. Sol. 28, 2067 (1967)

37. R. Ramirez and L.M. Falicov, Phys.Rev. B1, 3464 (1970)

38. N.O. Lipari, phys.stat.sol. 40, 691 (1970)

39. U. Rössler, phys.stat.sol. 42, 345 (1970)

40. N.O. Lipari and W.B. Fowler, Phys.Rev. B 2, 3354 (1970)

41. N.O. Lipari, A.B. Kunz, and W.B. Fowler, phys.stat.sol. (b) 45, K 43 (1971)

42. L. Dagens and F. Perrot, Phys.Rev. B 5, 641 (1972)

43. R.S. Knox, The Theory of Excitons, Solid State Phys. Suppl. 5, (Academic Press, New York London, 1963)

44. U. Rössler, in Computational Solid State Physics, editors F. Herman, N.W. Dalton, and T.R. Koehler (Plenum Press New York - London 1972) p. 161

45. U. Rössler, phys.stat.sol. (b) 45, 483 (1971)

46. G. Baldini and R.S. Knox, Phys.Rev. Letters 11, 127 (1963)
G. Baldini, Phys.Rev. 137, A508 (1965)
J.-Y. Roncin, N. Damany, and J. Romand, J.Mol.Spectr. 22, 154 (1967);
J.-Y. Roncin, V. Chandrasekharan, N. Damany, and B. Vodar, J.Chim.Phys. (France) 60, 1212 (1960)
47. N. Nagasawa, T. Karasawa, N. Miura, and T. Nanba, J.Phys.Soc. Japan 32, 1155(1972)
48. W. Martienssen, J.Phys.Chem.Sol. 2, 257 (1957)
H. Mahr, Phys.Rev. 122, 1464 (1961)
H. Saito, S. Saito, and R. Onaka, J.Phys.Soc. Japan 27, 126 (1969);
M. Watanabe, Y. Nakamura, Y. Nakai, and T. Murata, J.Phys.Soc. Japan 26, 1014 (1969)
49. Y. Nakamura, M. Watanabe, S. Sato, and Y. Nakai (unpublished)
50. J.A.R. Samson, Techniques of Vacuum Ultraviolet Spectroscopy (John Wiley & Sons, Inc., New York, 1967)
51. Unpublished DESY results
52. K. Codling and R.P.Madden, Phys.Rev. Letters 12, 106 (1964)
53. K. Codling, R.P. Madden, and D.L. Ederer, Phys.Rev. 155, 26 (1967)
54. A.I. Kozlenkov, Sov.Phys.-Dokl. 25, 957 (1961)
55. R. Kronig, Z. Phys. 70, 317 (1931) and 75, 191 (1932)
56. Y. Onodera and Y. Toyozawa, J.Phys.Soc. Japan 24, 341 (1968)
57. K. Codling and R.P. Madden, Appl.Opt. 4, 1431 (1965)

Table I: Energy positionsof the absorption maxima in the 4d spectrum of pure solid Xe and their maximum shift in Xe:Kr and Xe:Ar mixtures (as extrapolated for c_{Xe} = 0 % and $c_{Kr,Ar}$ = 100 %)

Peak	pure Xe (eV)	maximum shift in Xe:Kr mixtures (eV)	maximum shift in Xe:Ar mixtures (eV)
A	64.3 ±0.08	0.0 ± 0.1	0.0 ±0.06
B	65.35±0.05	+0.17 ± 0.05	+0.58±0.08
B'	67.34±0.05	+0.16 ± 0.05	+0.58±0.08
C	65.6 ±0.05	+0.28 ± 0.05	+0.75±0.1
C'	67.58±0.05	+0.25 ± 0.05	+0.80±0.1
D	66.0 ±0.1	+0.3 ± 0.1	
D'	68.0 ±0.07	+0.65 ± 0.15	
E,F	66.8 ±0.08	+0.55 ± 0.08	+2.2 ±0.4
E',F'	68.8 ±0.08	+0.42 ± 0.08	+2.5 ±0.4
G	70.0 ±0.05	+1.5 ± 0.15	+2.75±0.3
H	72.33±0.07	+2.02 ± 0.15	+3.2 ±0.3
H'	74.4 ±0.07	+2.04 ± 0.15	+3.2 ±0.3
I	76.45±0.08	+2.06 ± 0.15	+3.2 ±0.3
J	80.0 ±0.08	0.0 ± 0.08	

Table II: Energy positions of the absorption maxima in the 3d spectrum of pure solid Kr and their maximum shift in Kr:Xe and Kr:Ar mixtures (as extrapolated for c_{Kr} = 0 % and $c_{Xe,Ar}$ = 100 %)

Peak	pure Kr (eV)	maximum shift in Kr:Xe mixtures (eV)	maximum shift in Kr:Ar mixtures (eV)
A	90.4 ±0.08		
B	91.73±0.05	-0.14±0.1	+0.38±0.05
B'	93.00±0.05	-0.20±0.08	+0.37±0.05
C	92.08±0.05	-0.18±0.1	+0.48±0.05
C'	93.34±0.05	-0.21±0.1	+0.59±0.05
E	94.23±0.05	-0.7 ±0.1	+0.93±0.2
E'	95.45±0.08		+0.93±0.2
G	95.03±0.06	-0.8 ±0.25	+1.1 ±0.2
G'	96.4 ±0.06	-0.75±0.25	+0.9 ±0.2
H	95.85±0.07	-1.1 ±0.2	
H'	97.13±0.09	-1.1 ±0.2	
I	98.25±0.1		+1.1 ±0.3
J	98.8 ±0.1		+1.03±0.2 +2.04±0.3
K	101.05±0.1		+1.55±0.3
K'	102.4 ±0.15		+1.6 ±0.4
L	106.05±0.15		+0.4 ±0.4 +1.4 ±0.5
M	110.6 ±0.2		+0.45±0.4

Table III: Energy positions and relative distances of the first absorption lines in gaseous and solid Ne 2s, Ar 3s and 2p, Kr 3d, and Xe 4d transitions

	J	gas (eV)		solid (eV)	ΔE solid-gas (eV)	ΔE solid (eV)
Ne 2s	0	45.54±0.04	2s→3p	46.92±0.04 (A)	1.38±0.04 (A)	1.08±0.04 (B-A)
				48.0 ±0.04 (B)	2.46±0.04 (B)	
Ar 3s	0	26.61±0.02	3s→4p	27.52±0.02 (A)	0.91±0.02 (A)	0.48±0.02 (B-A)
				28.00±0.02 (B)	1.39±0.02 (B)	
Ar 2p	$\frac{3}{2}$	2.44.4±0.15	2p→4s	245.2 ±0.2 (A)	0.8 ±0.2	
	$\frac{1}{2}$	246.5 ±0.15	2p'→4s'	247.35±0.2 (A')	0.85±0.2	
Kr 3d	$\frac{5}{2}$	91.22±0.07	3d→5p	91.73±0.05 (B)	0.51±0.07 (B)	0.35±0.05 (C-B)
				92.08±0.05 (C)	0.86±0.07 (C)	
	$\frac{3}{2}$	92.44±0.07	3d'→5p	93.00±0.05 (B')	0.56±0.07 (B')	0.34±0.05 (C'-B')
				93.34±0.05 (C')	0.9 ±0.07 (C')	
Xe 4d	$\frac{5}{2}$	65.10±0.02	4d→6p	65.35±0.05 (B)	0.25±0.05 (B)	0.25±0.05 (C-B)
				65.6 ±0.05 (C)	0.5 ±0.05 (C)	
	$\frac{3}{2}$	67.02±0.02	4d'→6p'	67.34±0.05 (B')	0.32±0.05 (B')	0.24±0.05 (C'-B')
				67.58±0.05 (C')	0.56±0.05 (C')	

Figure Captions

Fig. 1 Absorption curves of the pure solid rare gases Ne, Ar, Kr, and Xe compiled from the data given in ref.s 1-4. The energy ranges are indicated where the fine structure of the different solid rare gases have been studied with alloying of other rare gases and N_2.

Fig. 2 Fine structure of the Xe 4d absorption in the energy range 64 to 90 eV for different Xe:Kr mixtures ranging from 100 % to 1 % Xe. The corresponding peaks are connected by dashed lines.

Fig. 3 Position of the different absorption peaks A to J in the Xe 4d spectrum for different concentrations of Xe:Kr mixtures.

Fig. 4 Fine structure of the Kr 3d absorption in the energy range 90 to 99 eV for different Kr:Xe mixtures ranging from 100 % to 10 % Kr. The curve for 100 % Xe is also included to explain the continuum absorption increasing towards higher photon energies for small Kr concentrations.

Fig. 5 Position of the different absorption peaks B to H' in the Kr 3d spectrum for different concentrations of Kr:Xe mixtures.

Fig. 6 Fine structure of the Xe 4d absorption in the energy range 64 to 80 eV for different Xe:Ar mixtures ranging from 100 % to 10 % Xe. The corresponding peaks are connected by dashed lines.

Fig. 7 Fine structure of the Kr 3d absorption in the energy range 91 to 94.5 eV for different Kr:N_2 mixtures ranging from 100 % to 10 % Kr. The curve for pure N_2 is also included. The dashed lines connect peaks in the alloy system, the dotted lines in the decomposed system.

Fig. 8 Fine structure of the Kr 3d absorption in the energy range 90 to 99 eV for different Kr:Ar mixtures ranging from 100 % to 5 % Kr. The corresponding peaks are connected by dashed lines.

Fig. 9 Fine structure of the Ar 2p absorption in the energy range 243 to 255 eV for different Ar:N_2 mixtures ranging from 100 % to 10 % Ar.

Fig. 10 Fine structure of the Ne 2s absorption in the energy range 45.5 to 48.5 eV for different Ne:Ar mixtures ranging from 100 % to 40 % Ne.

Fig. 11 The first absorption lines in gaseous (dashed lines) and solid (solid lines) Ne near the 2s threshold, Ar near the 3s and 2p thresholds, Kr near the 3d threshold and Xe near the 4d threshold.

Fig. 12 Energy distance between the first solid state absorption lines and the corresponding lines in the gas for Xe 4d, Kr 3d, Ar 3s and 2p, and Ne 2s transitions in the pure solids and in alloys with the other rare gases.

Fig. 13 Energy distance between the first two solid state absorption lines for Xe 4d, Kr 3d, Ar 3s,and Ne 2s transitions in the pure solid and in alloys with the other rare gases.

Fig. 14 Plot of the averaged energy distance from Fig.s 12 and 13 versus $\frac{1}{a^2}$ a being the lattice parameter.

Fig. 15 Density of states of the conduction bands of solid Ar, Kr and Xe (essentially taken from ref. 45, the results of Xe differ from those in ref. 45, where the third and fourth conduction bands on the Σ axis are incorrect in comparison to the results of ref. 39).

Fig. 16 Diagram showing the relative positions of corresponding maxima of the density of states of the conduction bands of solid Xe and Kr and the shift of the experimental peaks of Xe and Kr when alloying the other gas.

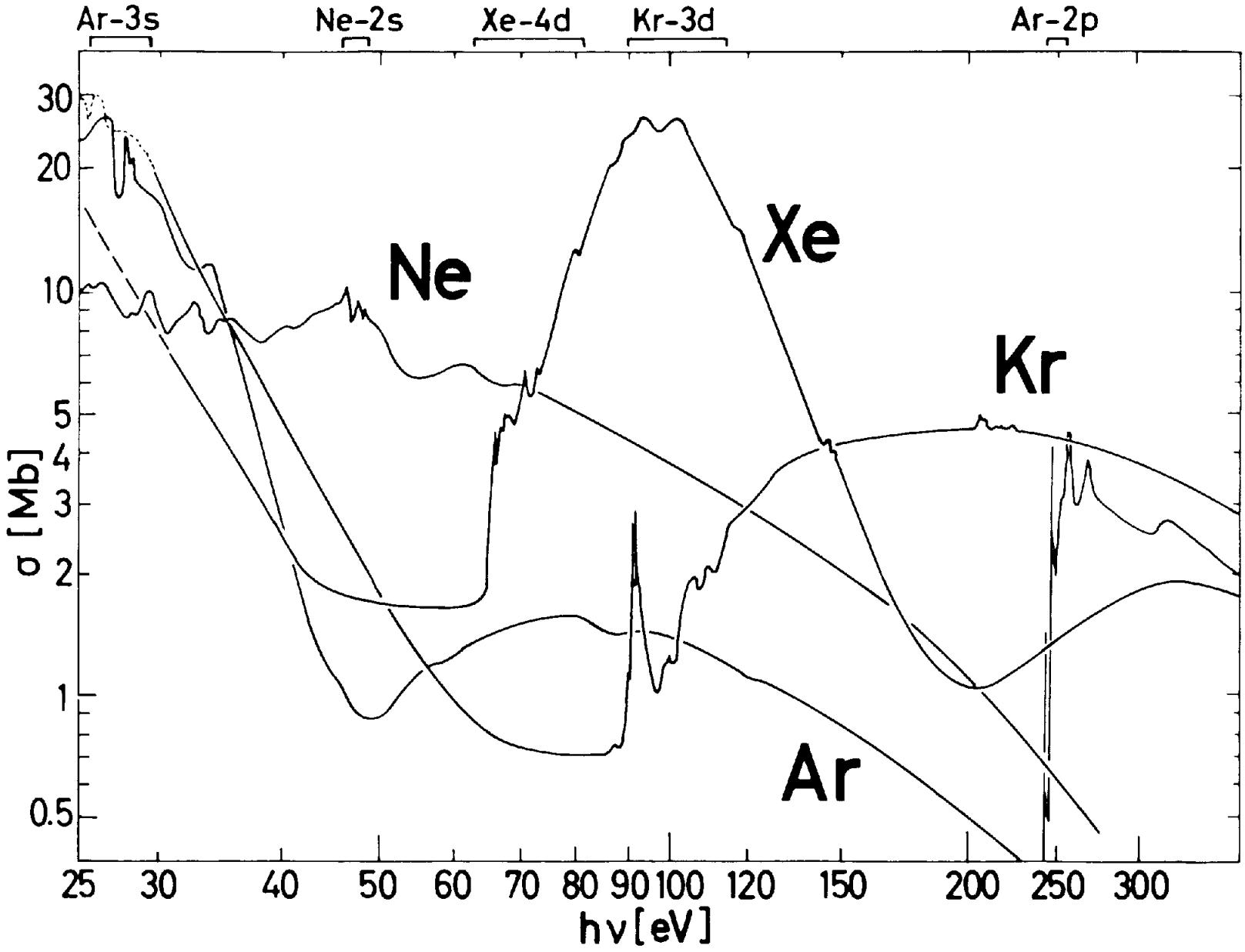
Ar-3s
Ne-2s
Xe-4d
Kr-3d
Ar-2p
Ne
Xe
Kr
Ar
σ [Mb]
30
20
10
5
4
3
2
1
0.5
25
30
40
50
60
70
80
90
100
120
150
200
250
300
hν [eV]

Fig. 1

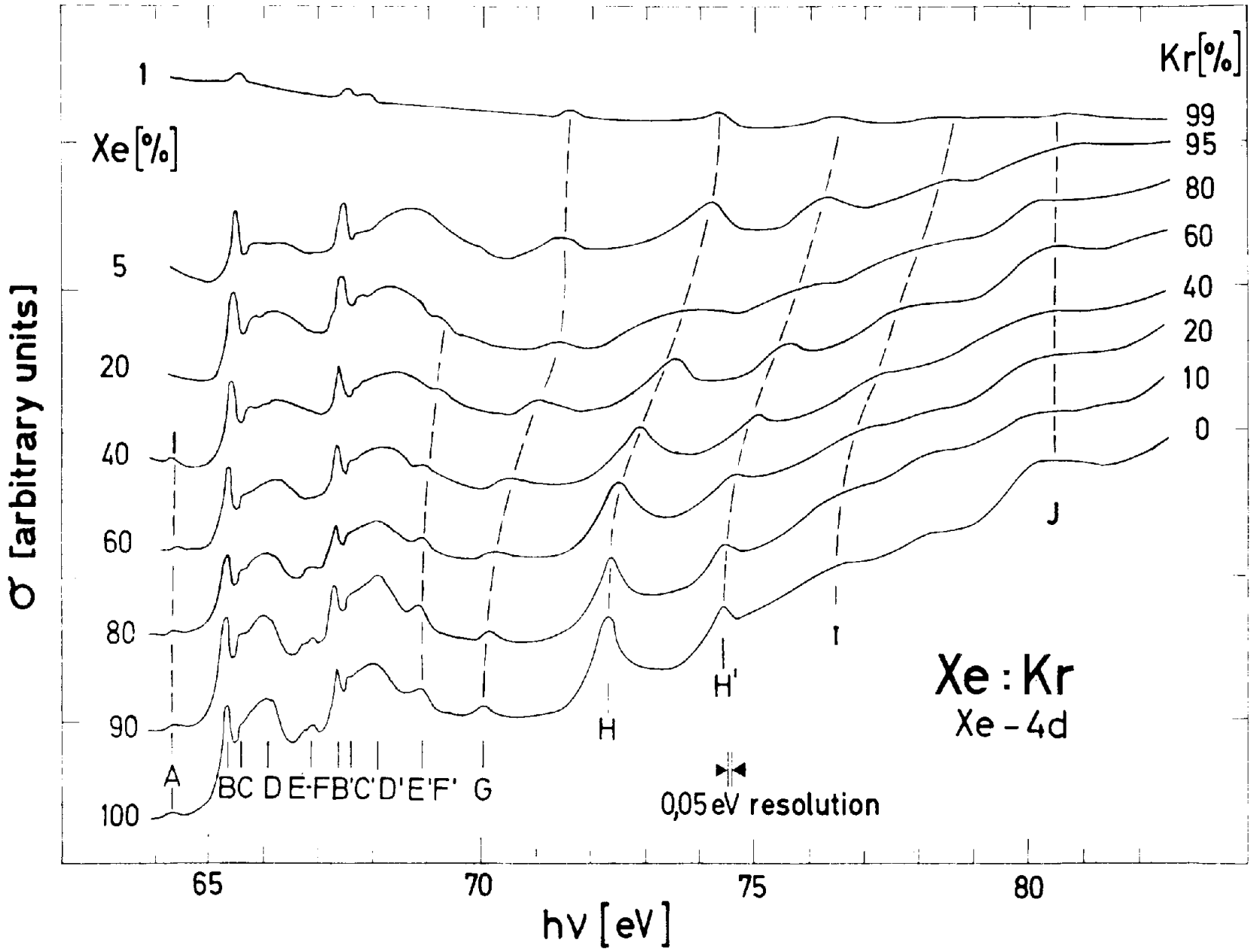
Kr[%]
1
99
95
80
60
40
20
10
0
Xe[%]
5
20
40
60
80
90
100
σ [arbitrary units]
A
BC D E-F B'C' D' E' F' G
H
H'
I
J
Xe : Kr
Xe - 4d
0,05 eV resolution
65
70
75
80
hν [eV]

Fig. 2

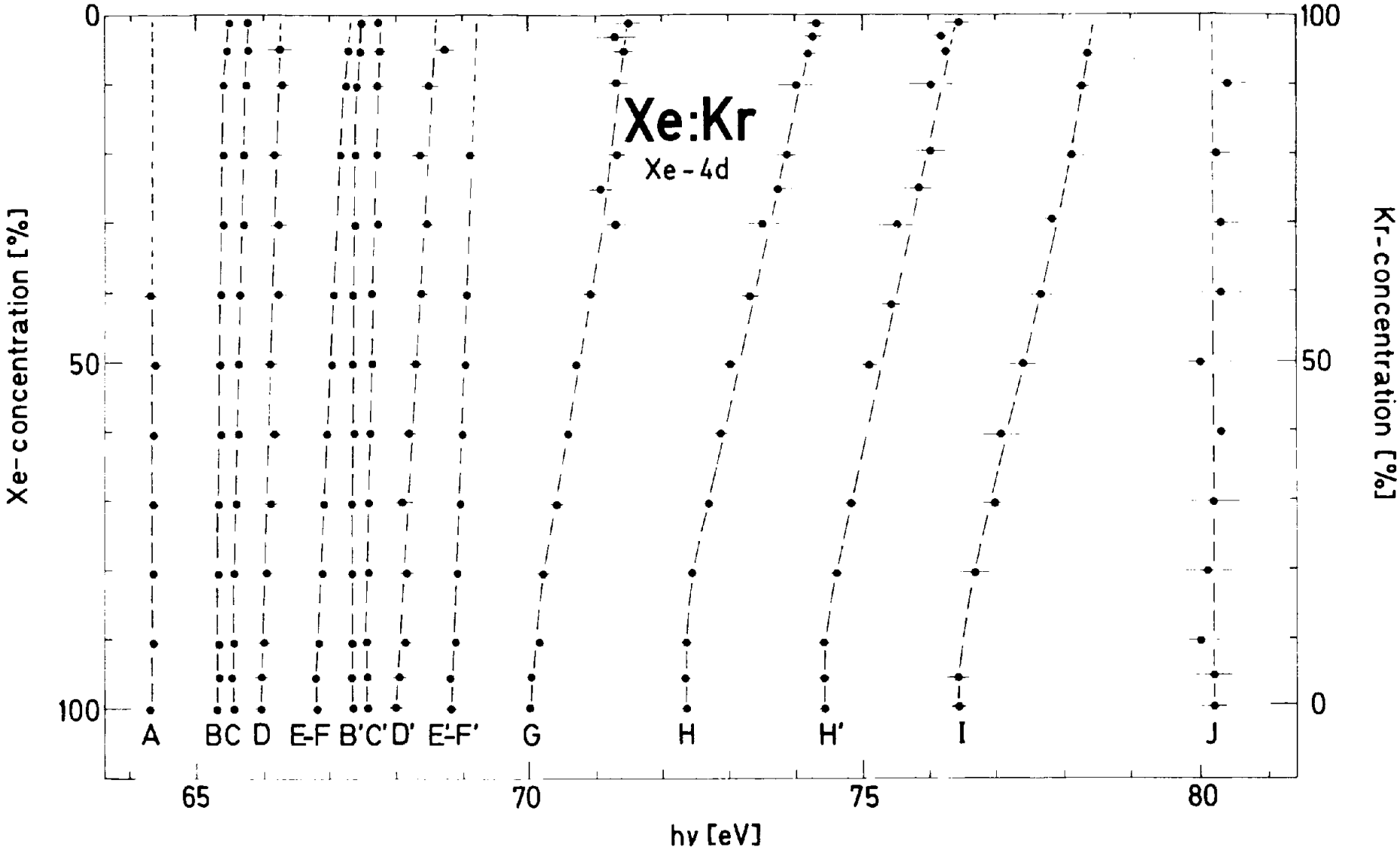
Xe:Kr
Xe - 4d
Xe-concentration [%]
Kr-concentration [%]
0
50
100
A
BC
D
E-F
B'C'
D'
E'-F'
G
H
H'
I
J
65
70
75
80
hν [eV]

Fig. 3

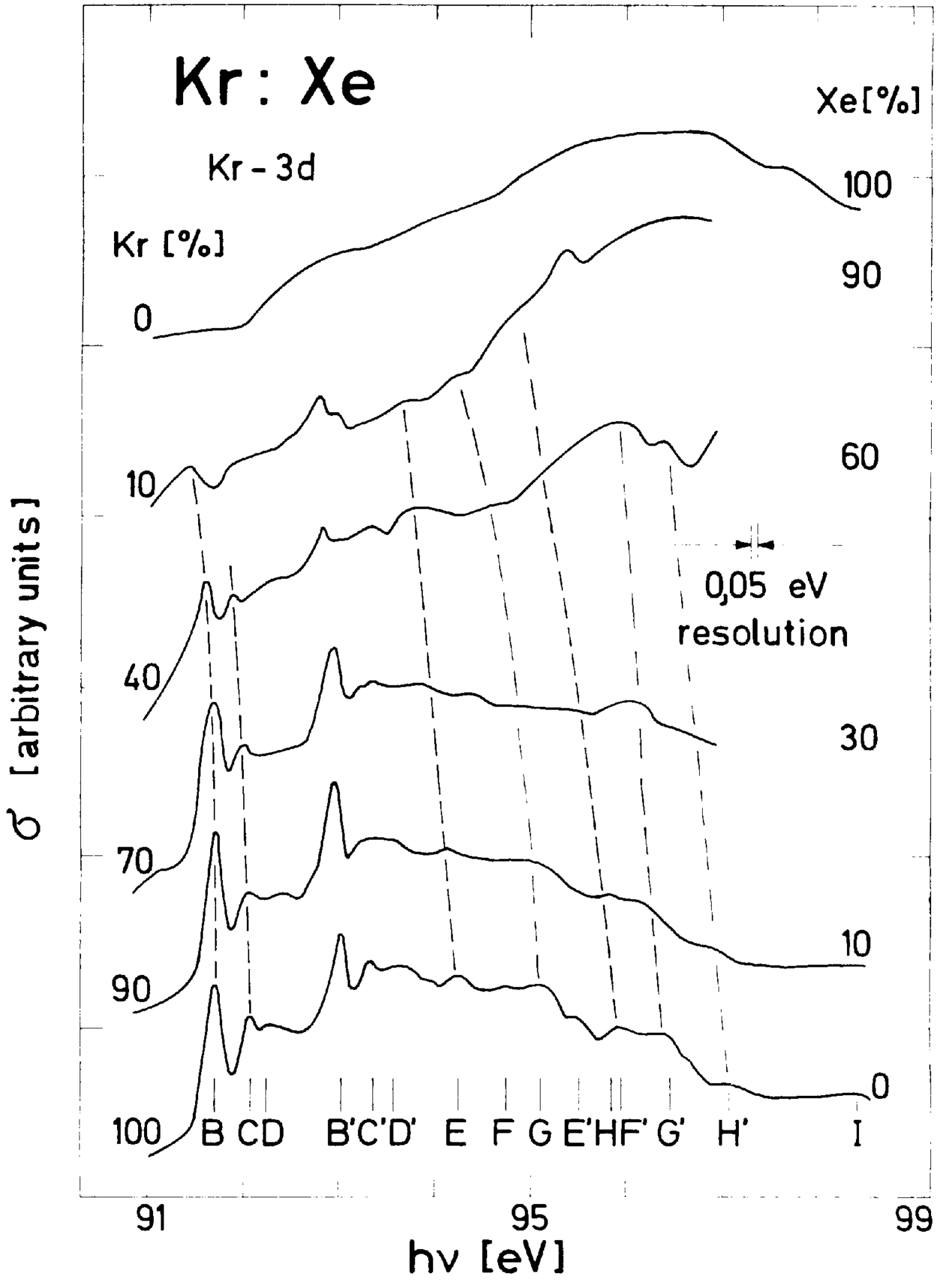
Kr : Xe
Kr - 3d
Kr [%]
0
10
40
70
90
100
Xe[%]
100
90
60
30
10
0
0,05 eV
resolution
B C D B' C' D' E F G E' H F' G' H' I
91
95
99
hν [eV]
σ [arbitrary units]

Fig. 4

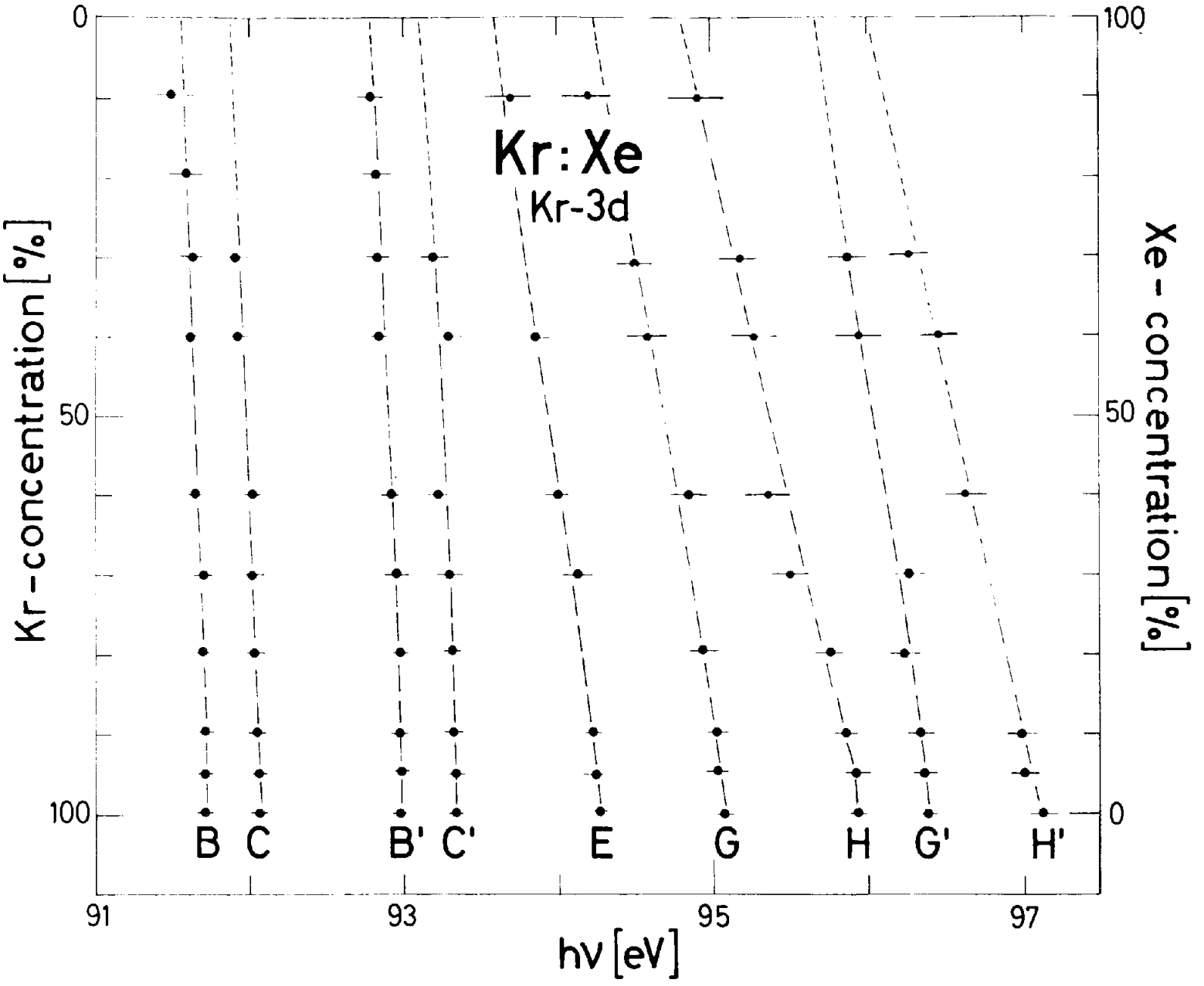
Kr:Xe
Kr-3d
Kr-concentration [%]
Xe-concentration [%]
0
50
100
100
50
0
B
C
B'
C'
E
G
H
G'
H'
91
93
95
97
hν [eV]

Fig. 5

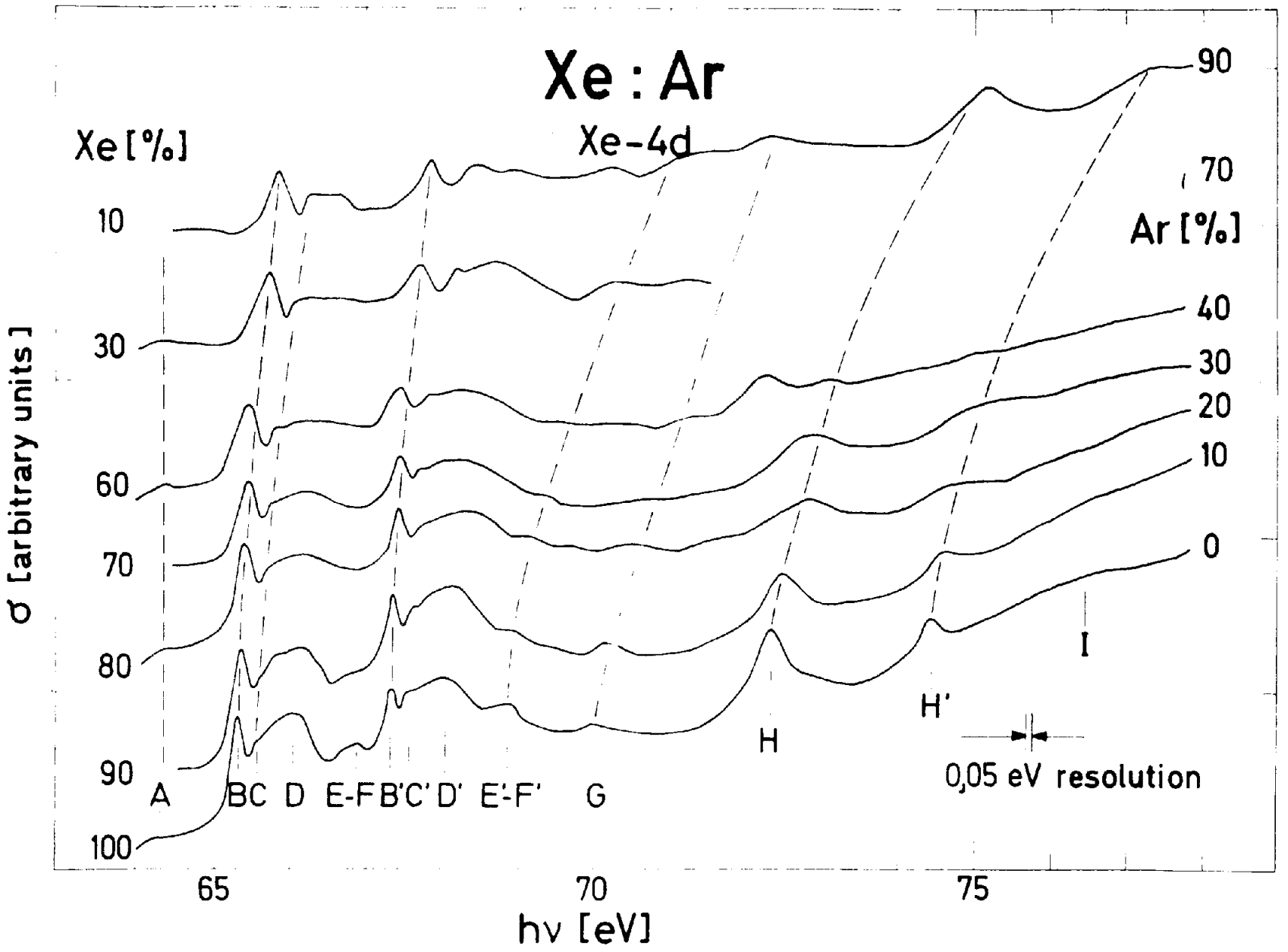
Xe : Ar
Xe-4d
Xe [%]
10
30
60
70
80
90
100
Ar [%]
90
70
40
30
20
10
0
σ [arbitrary units]
A
BC
D
E-F
B'C'
D'
E'-F'
G
H
H'
I
0,05 eV resolution
65
70
75
hν [eV]

Fig. 6

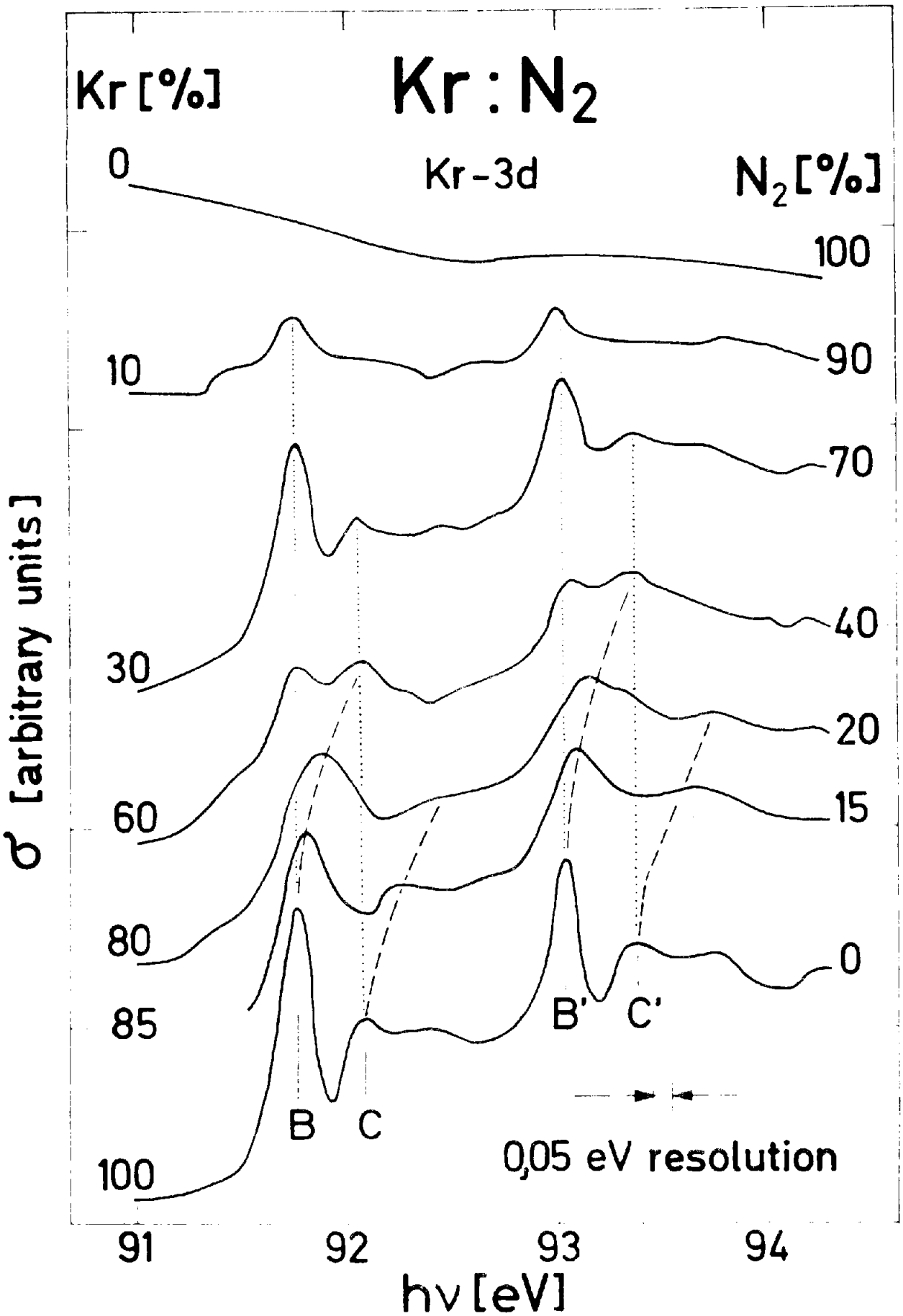
Kr [%]
Kr : N2
Kr-3d
N2 [%]
0
100
10
90
70
30
40
60
20
15
80
0
85
B'
C'
B
C
100
0,05 eV resolution
σ [arbitrary units]
91
92
93
94
hν [eV]

Fig. 7

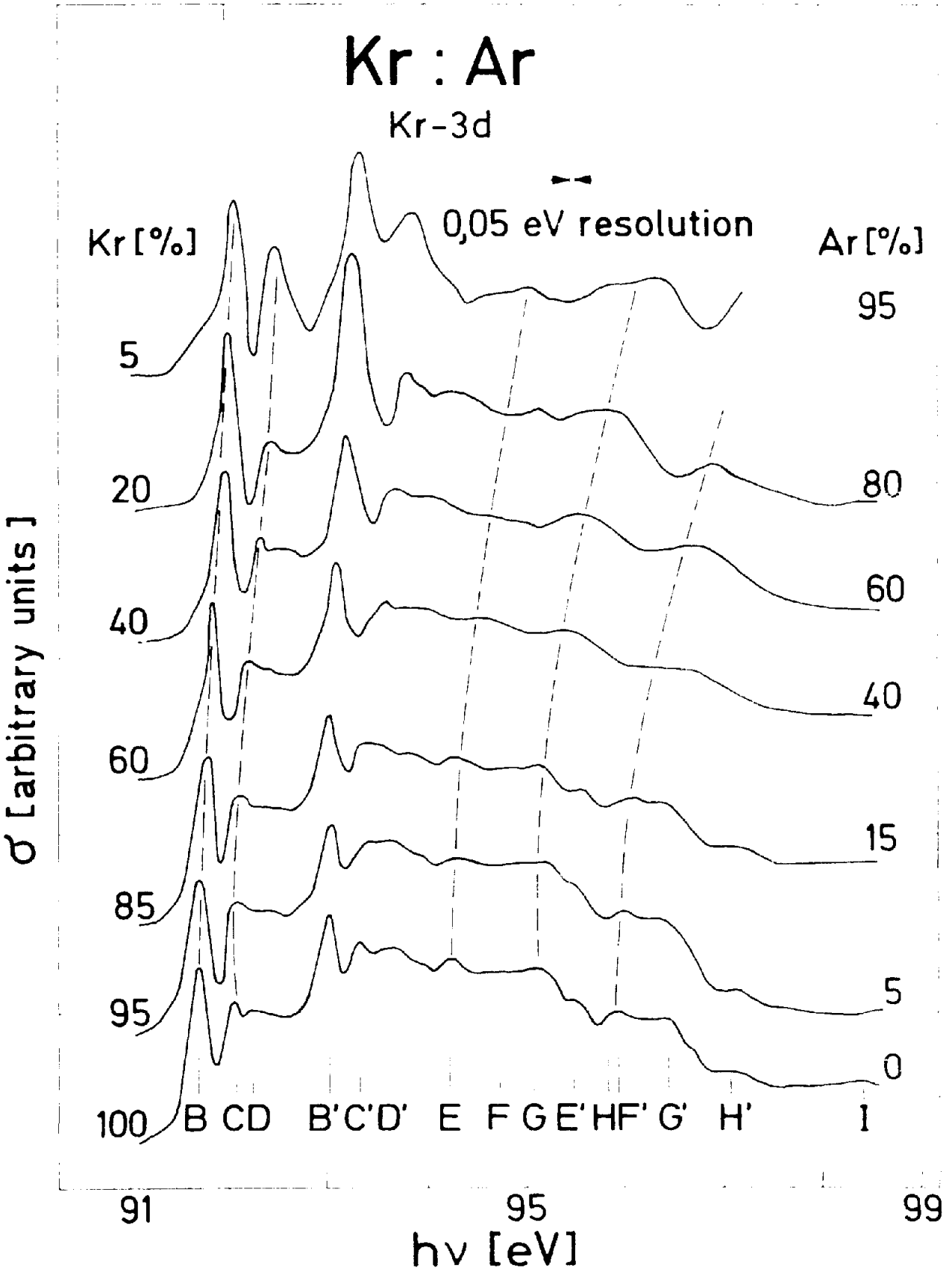
Kr : Ar
Kr-3d
0,05 eV resolution
Kr [%]
Ar [%]
5
95
20
80
40
60
60
40
85
15
95
5
100
0
B CD B'C'D' E F G E' HF' G' H' I
σ [arbitrary units]
91
95
99
hν [eV]

Fig. 8

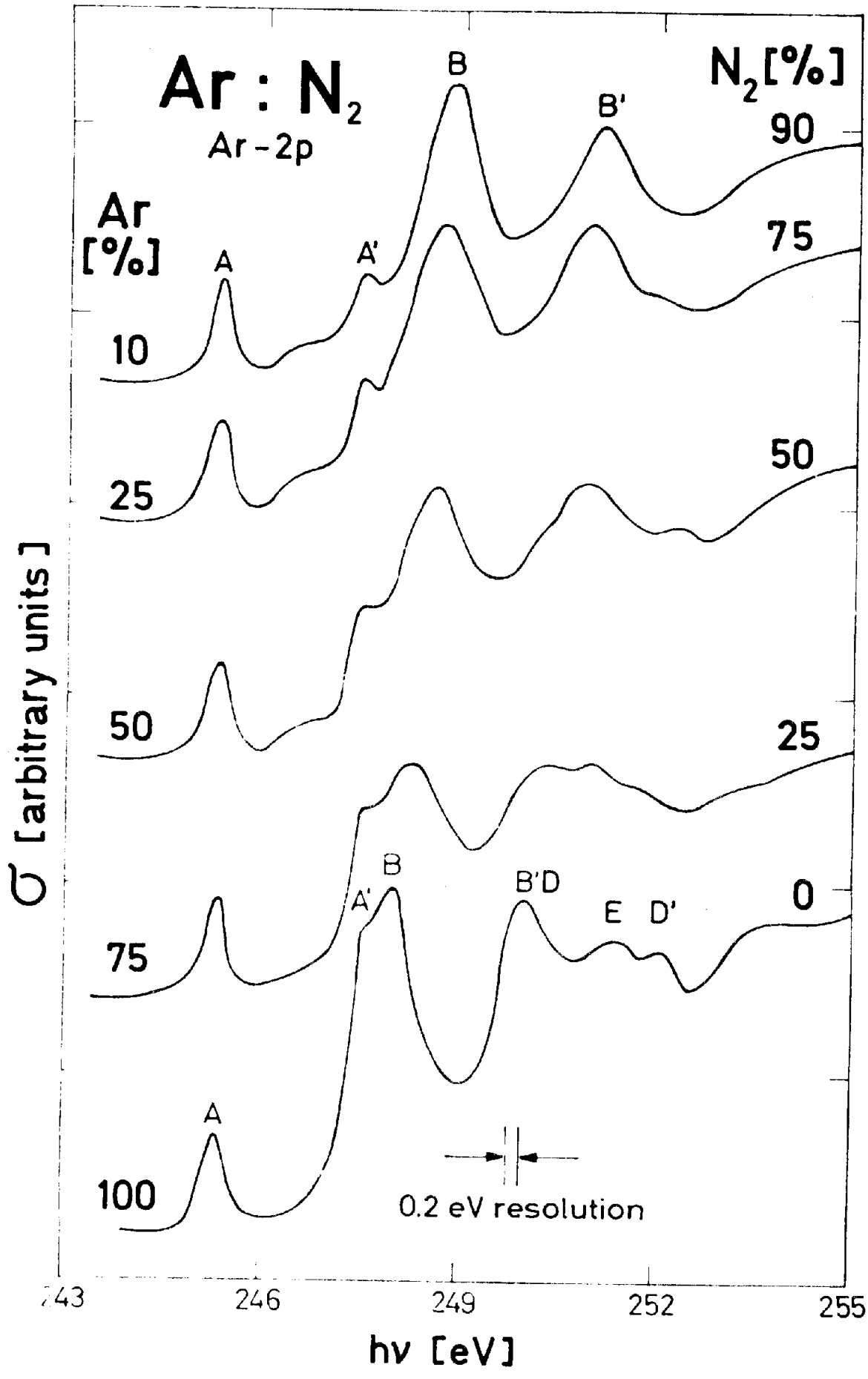
Ar : N2
Ar-2p
N2[%]
Ar [%]
90
75
50
25
0
10
25
50
75
100
A
A'
B
B'
B'D
E
D'
0.2 eV resolution
σ [arbitrary units]
243
246
249
252
255
hν [eV]

Fig. 9

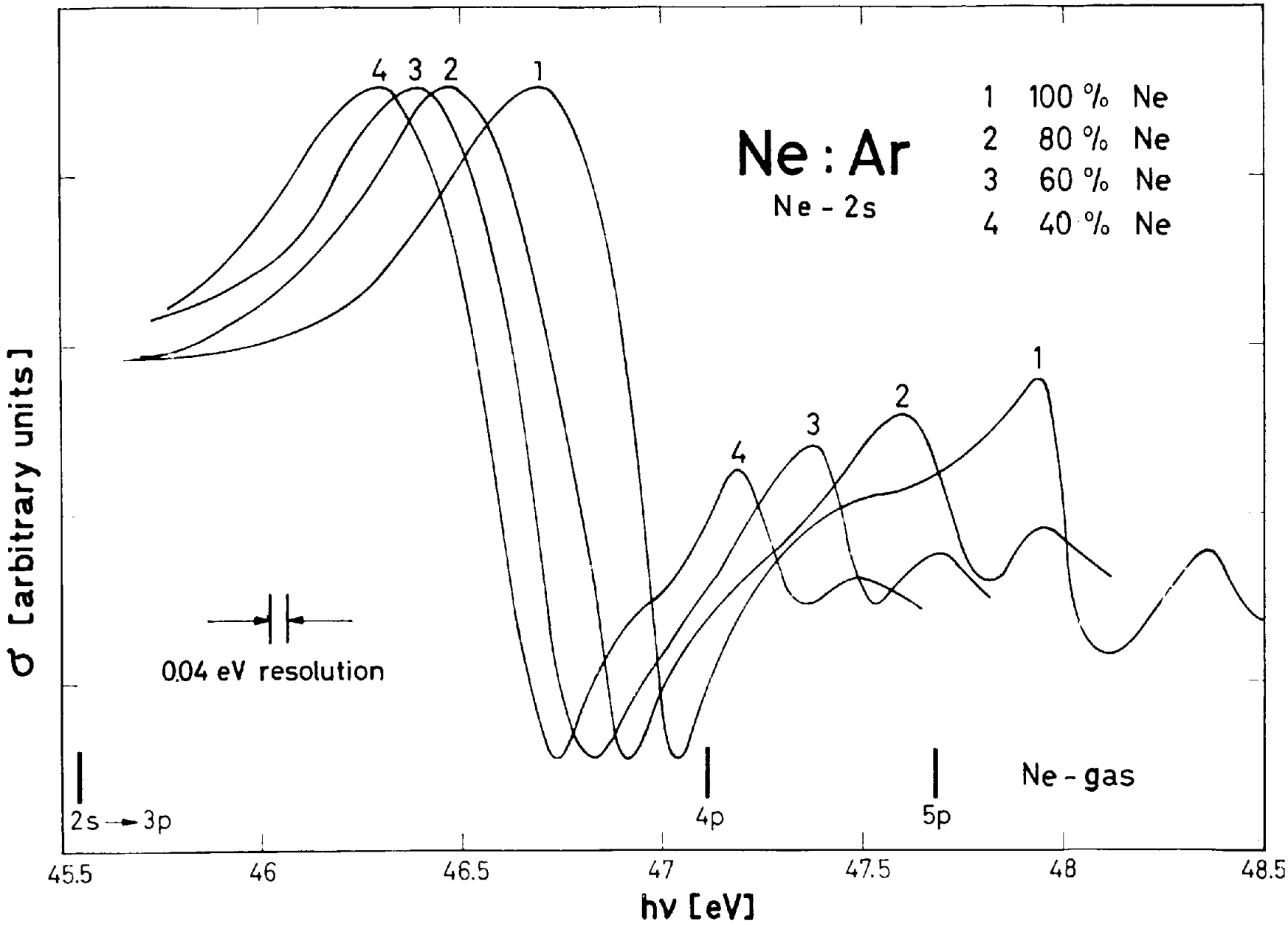
Ne : Ar
Ne - 2s
1 100 % Ne
2 80 % Ne
3 60 % Ne
4 40 % Ne
4 3 2 1
1
2
3
4
0.04 eV resolution
2s → 3p
4p
5p
Ne - gas
σ [arbitrary units]
45.5
46
46.5
47
47.5
48
48.5
hν [eV]

Fig.10

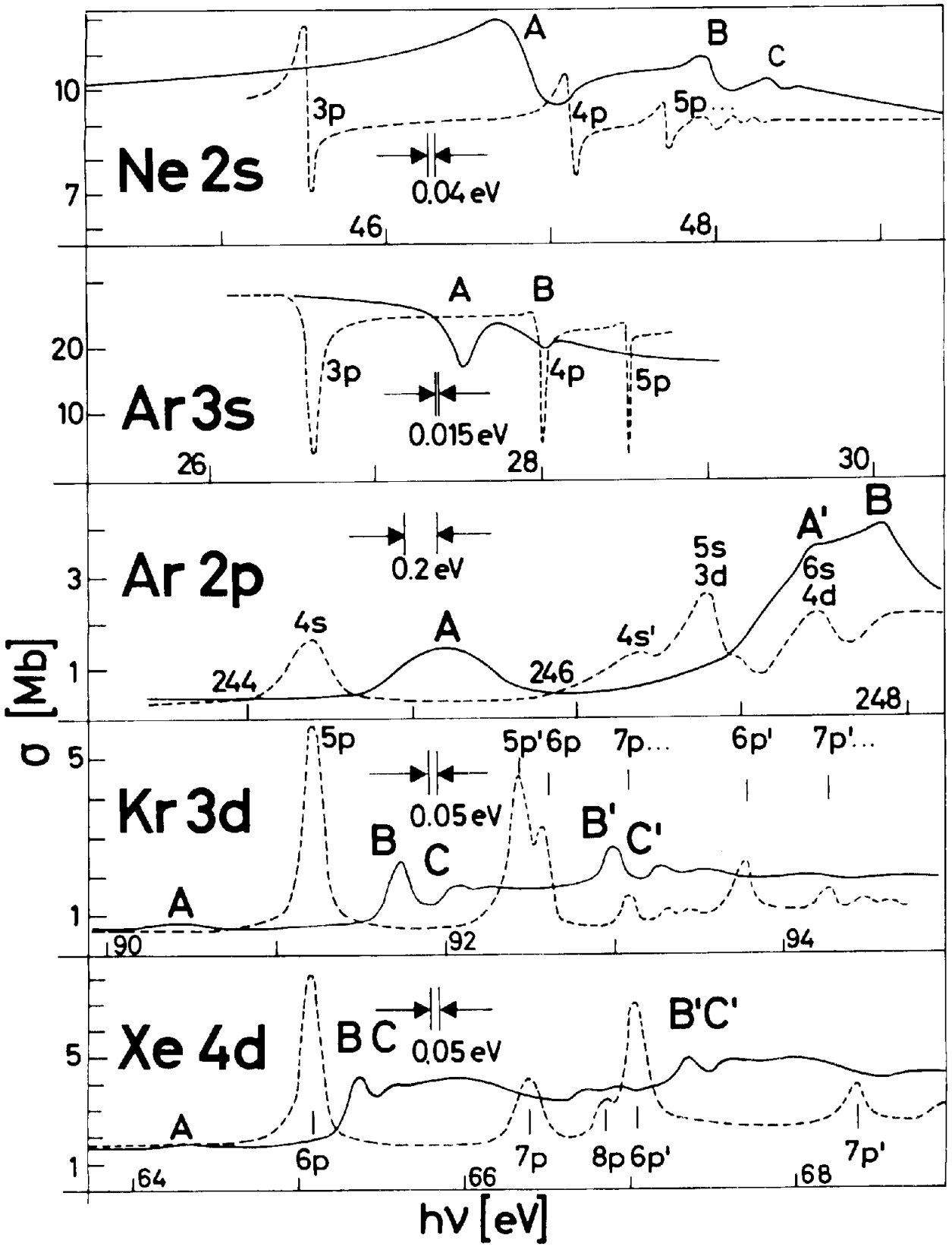
Ne 2s
A
B
C
3p
4p
5p
0.04 eV
10
7
46
48
Ar 3s
A
B
3p
4p
5p
0.015 eV
20
10
26
28
30
Ar 2p
0.2 eV
4s
A
4s'
5s
3d
A'
B
6s
4d
3
1
244
246
248
Kr 3d
5p
5p'6p
7p...
6p'
7p'...
0.05 eV
B
C
B'
C'
A
5
1
90
92
94
Xe 4d
B C
0.05 eV
B'C'
A
6p
7p
8p 6p'
7p'
5
1
64
66
68
σ [Mb]
hν [eV]

Fig. 11

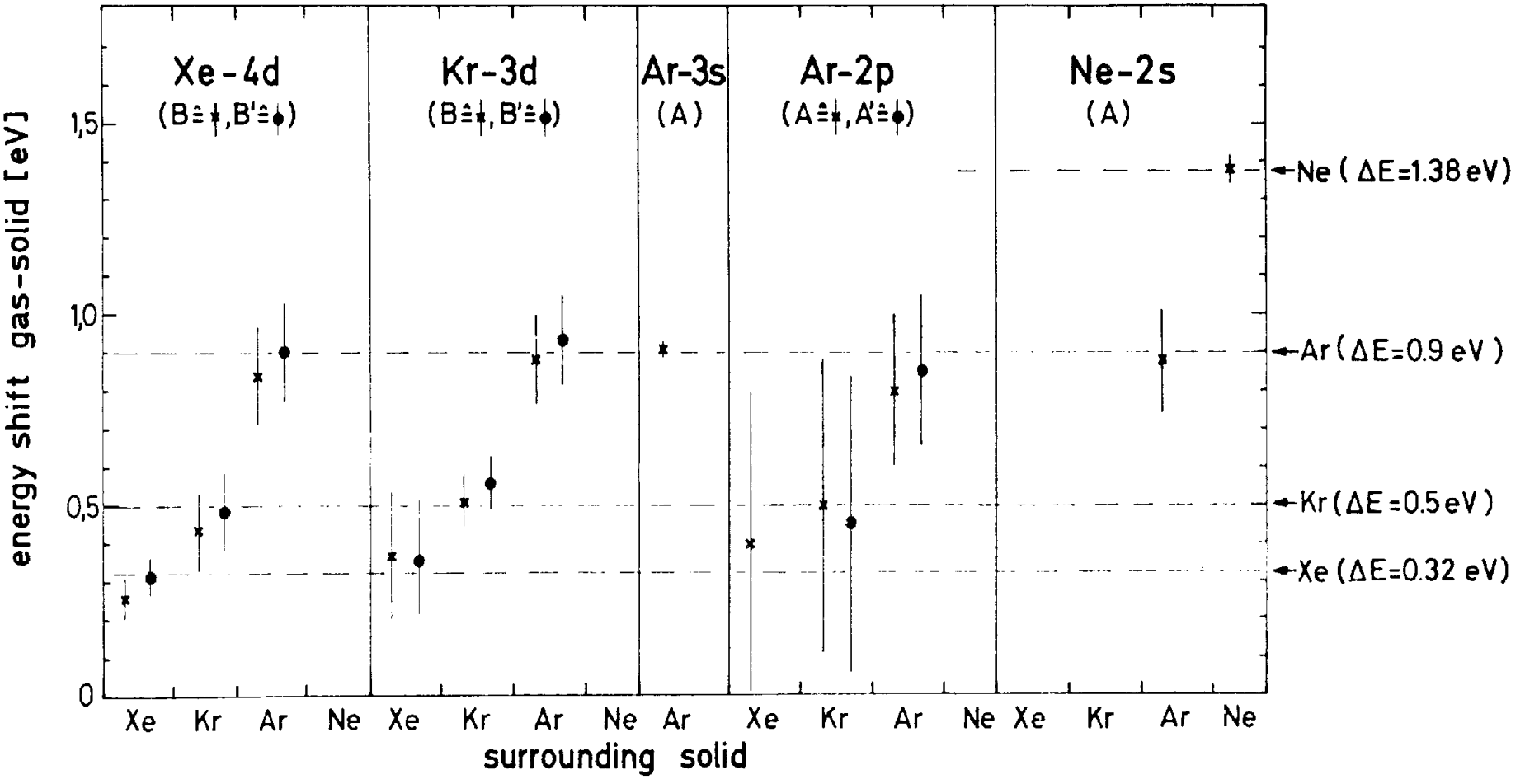
Xe-4d
(B≙↓, B'≙●)
Kr-3d
(B≙↓, B'≙●)
Ar-3s
(A)
Ar-2p
(A≙↓, A'≙●)
Ne-2s
(A)
energy shift gas-solid [eV]
1,5
1,0
0,5
0
Ne (ΔE=1.38 eV)
Ar (ΔE=0.9 eV)
Kr (ΔE =0.5 eV)
Xe (ΔE=0.32 eV)
Xe Kr Ar Ne Xe Kr Ar Ne Ar Xe Kr Ar Ne Xe Kr Ar Ne
surrounding solid

Fig. 12

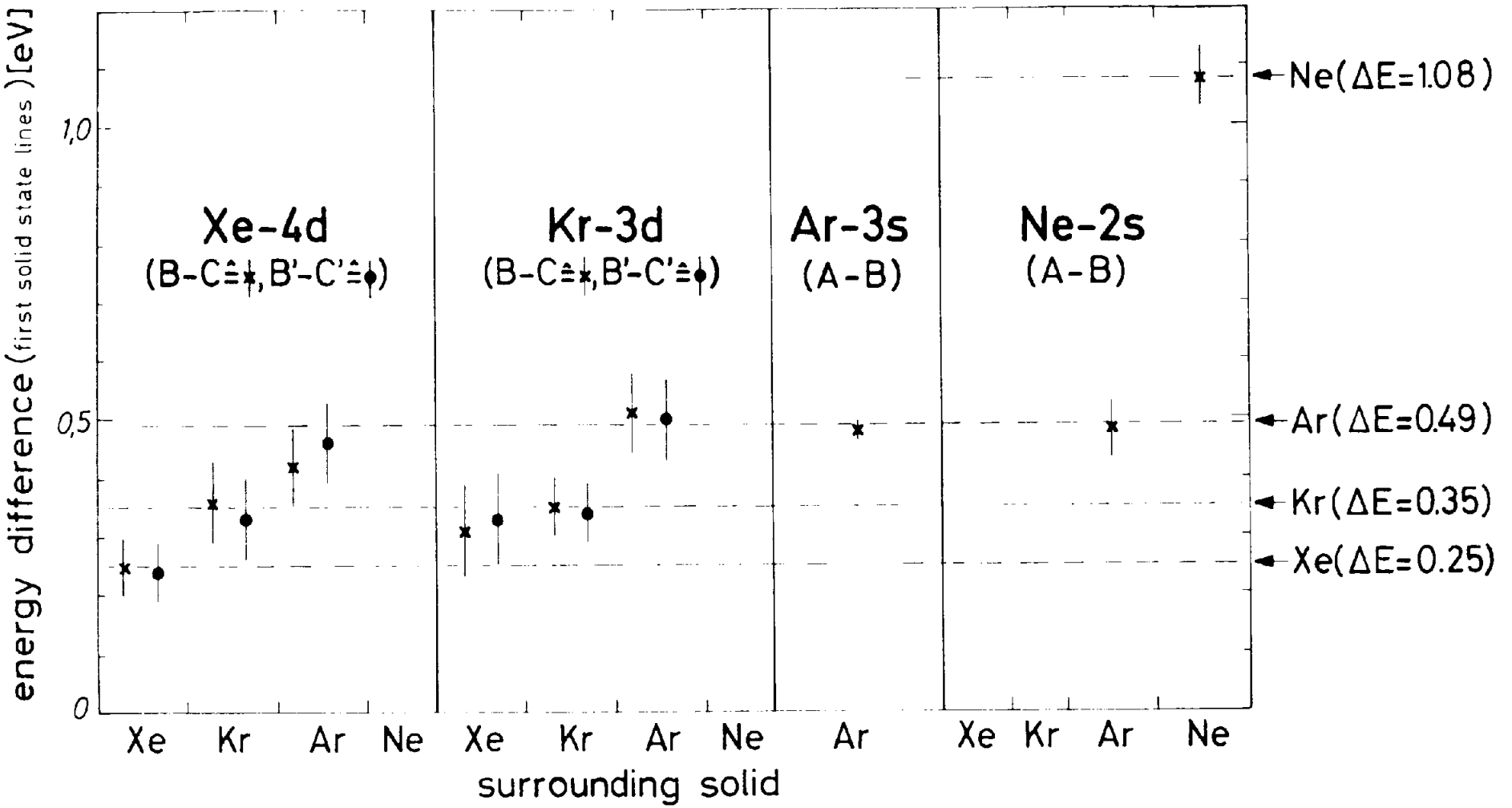
energy difference (first solid state lines) [eV]
1,0
0,5
0
Xe-4d
(B-C≙✱, B'-C'≙●)
Kr-3d
(B-C≙✱, B'-C'≙●)
Ar-3s
(A-B)
Ne-2s
(A-B)
Ne(ΔE=1.08)
Ar(ΔE=0.49)
Kr(ΔE=0.35)
Xe(ΔE=0.25)
Xe Kr Ar Ne Xe Kr Ar Ne Ar Xe Kr Ar Ne
surrounding solid

Fig. 13

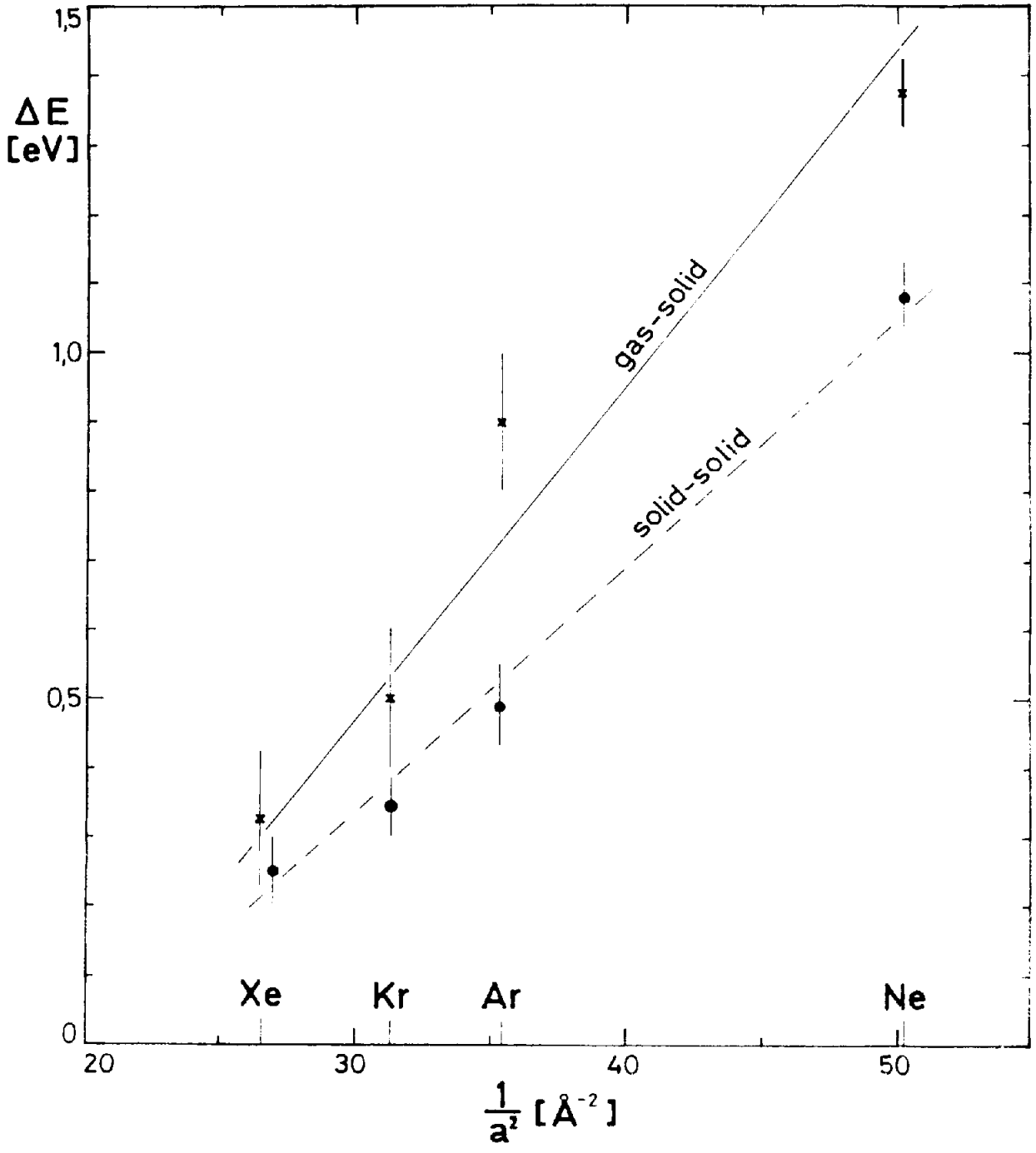
1,5
ΔE
[eV]
1,0
0,5
0
gas-solid
solid-solid
Xe
Kr
Ar
Ne
20
30
40
50
1/a² [Å⁻²]

Fig. 14

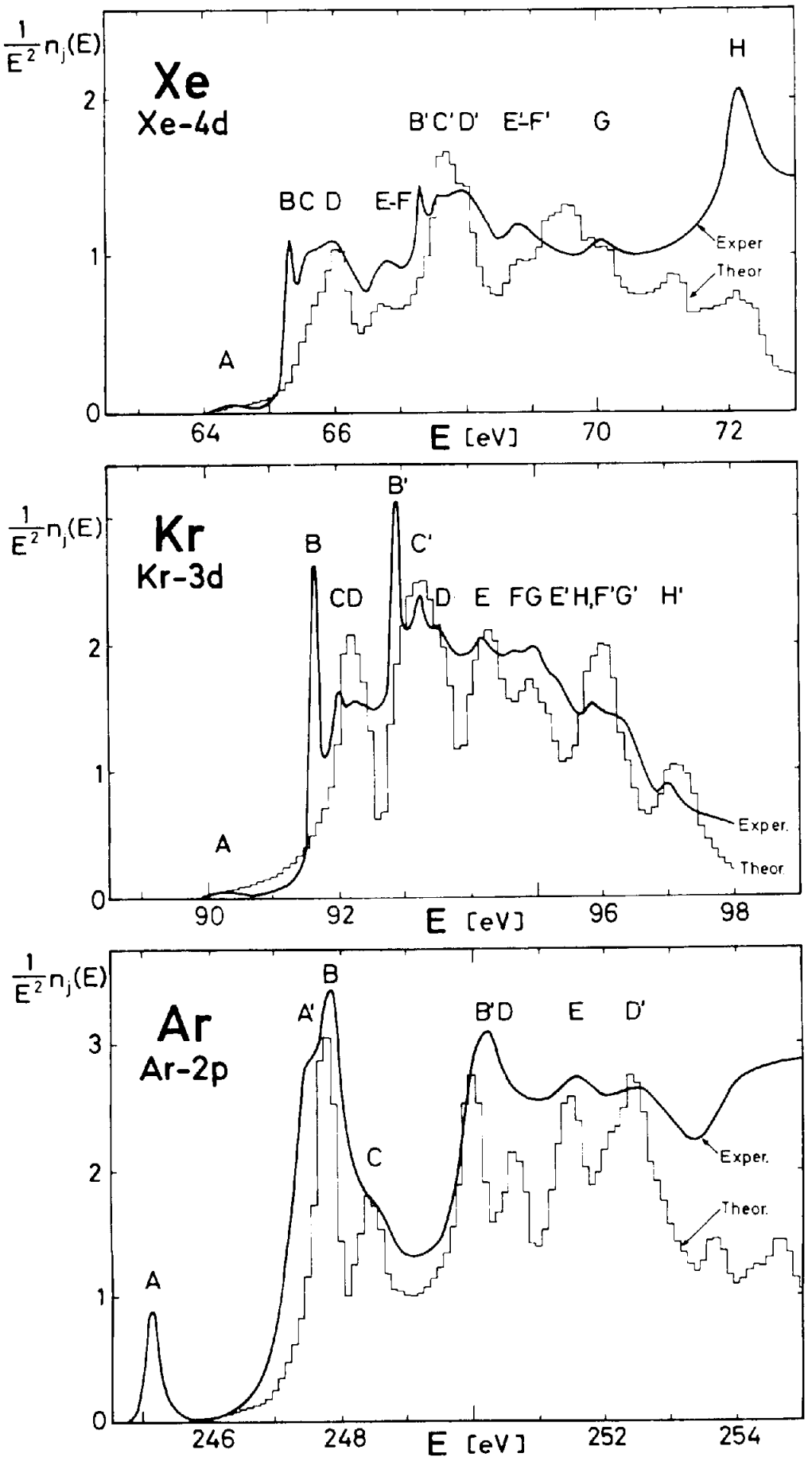
Xe
Xe-4d
$\frac{1}{E^2}n_j(E)$
A
BC D
E-F
B'C'D'
E-F'
G
H
Exper
Theor
64
66
E [eV]
70
72
Kr
Kr-3d
A
B
CD
B'
C'
D
E
FG
E'H,F'G'
H'
Exper.
Theor.
90
92
E [eV]
96
98
Ar
Ar-2p
A
A'
B
C
B'D
E
D'
Exper.
Theor.
246
248
E [eV]
252
254

Fig. 15

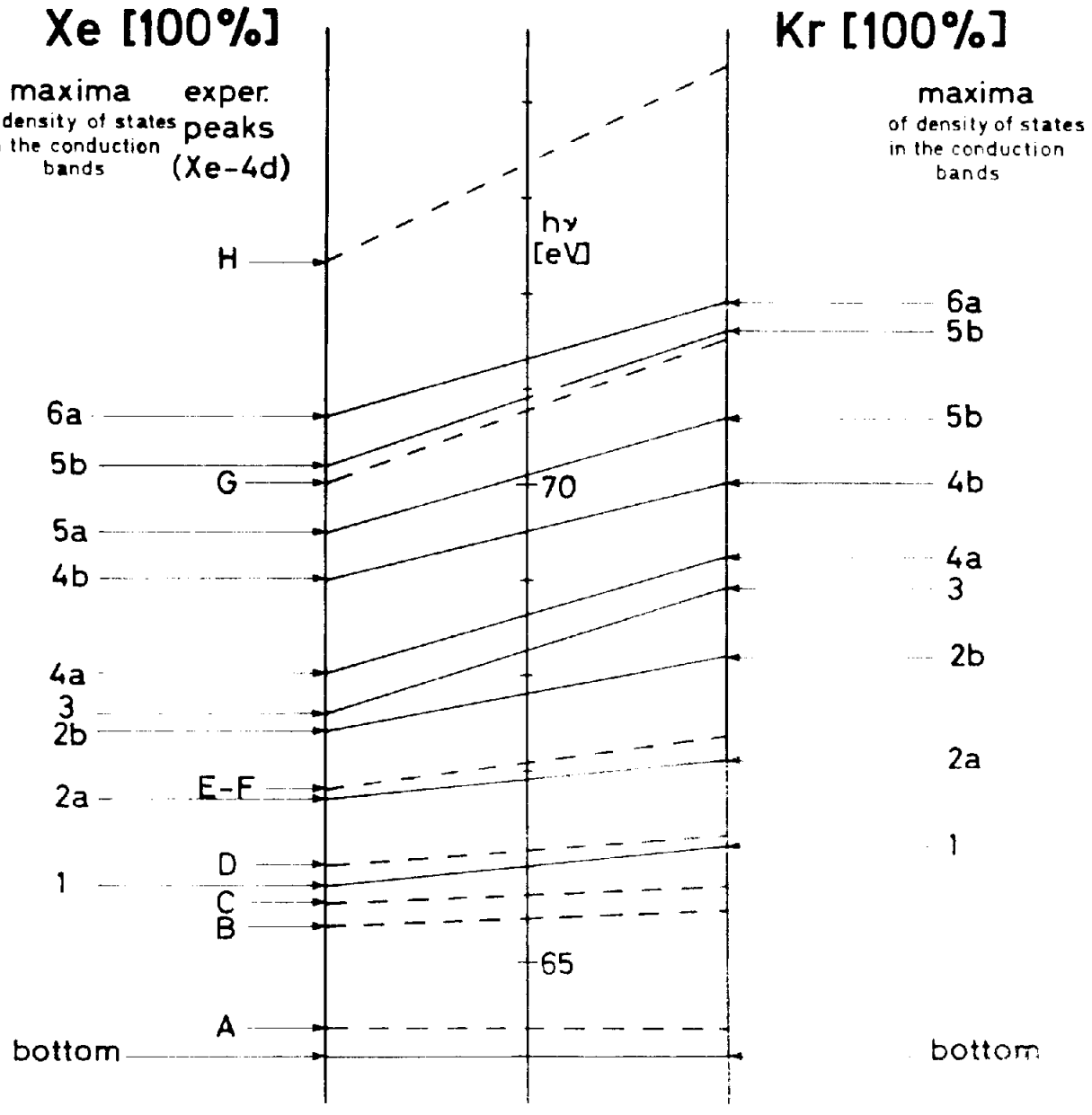
Xe [100%]
maxima of density of states in the conduction bands
exper. peaks (Xe-4d)
Kr [100%]
maxima of density of states in the conduction bands
hν [eV]
H
6a
5b
G
5a
4b
4a
3
2b
2a
E-F
1
D
C
B
A
bottom
70
65
6a
5b
5b
4b
4a
3
2b
2a
1
bottom

Fig. 16